Bioorganic Chemistry 103 (2020) 104186

Contents lists available at ScienceDirect

Bioorganic Chemistry

journal homepage: www.elsevier.com/locate/bioorg

Design, synthesis, biological evaluation, and docking study of novel dual-acting thiazole-pyridiniums inhibiting acetylcholinesterase and β-amyloid aggregation for Alzheimer's disease

Golaleh Ghotbi[a,b,c], Mohammad Mahdavi[d], Zahra Najafi[e], Farshad Homayouni Moghadam[f], Maryam Hamzeh-Mivehroud[b,c], Soodabeh Davaran[c,g], Siavoush Dastmalchi[b,c,h,*]

[a] Pharmaceutical Analysis Research Center, Tabriz University of Medical Sciences, Tabriz, Iran
[b] Biotechnology Research Center, Tabriz University of Medical Sciences, Tabriz, Iran
[c] Department of Medicinal Chemistry, School of Pharmacy, Tabriz University of Medical Sciences, Tabriz, Iran
[d] Endocrinology & Metabolism Research Institute (EMRI), Tehran University of Medical Sciences, Tehran, Iran
[e] Department of Medicinal Chemistry, School of Pharmacy, Hamadan University of Medical Sciences, Hamadan, Iran
[f] Department of Cellular Biotechnology, Cell Science Research Center, Royan Institute for Biotechnology, ACECR, Isfahan, Iran
[g] Drug Applied Research Center, Tabriz University of Medical Sciences, Tabriz, Iran
[h] Faculty of Pharmacy, Near East University, POBOX:99138, Nicosia, North Cyprus, Mersin 10, Turkey

ARTICLE INFO

Keywords:
Alzheimer's disease
Acetylcholinesterase
Docking study
Thiazole-pyridinium
Neuroprotection
β-amyloid self-aggregation

ABSTRACT

New compounds containing thiazole and pyridinium moieties were designed and synthesized. The potency of the synthesized compounds as selective inhibitors of acetylcholinesterase (AChE), and β-amyloid aggregation (Aβ) was evaluated. Compounds **7d** and **7j** showed the best AChE inhibitory activities at the submicromolar concentration range (IC_{50} values of 0.40 and 0.69 μM, respectively). Most of the novel compounds showed moderate to low inhibition of butyrylcholinesterase (BChE), which is indicative of their selective inhibitory effects towards AChE. Kinetic studies using the most potent compounds **7d** and **7j** confirmed a mixed-type of AChE inhibition mechanism in accordance with the docking results, which shows their interactions with both catalytic active (CAS) and peripheral anionic (PAS) sites. The specific binding of **7a**, **7j**, and **7m** to PAS domain of AChE was also confirmed experimentally. In addition, **7d** and **7j** were able to show β-amyloid self-aggregation inhibitory effects (20.38 and 42.66% respectively) stronger than donepezil (14.70%) assayed at 10 μM concentration. Moreover, compounds **7j** and **7m** were shown to be effective neuroprotective agents in H_2O_2-induced oxidative stress on PC_{12} cells almost similar to those observed for donepezil. The ability of **7j** to pass blood-brain barrier was demonstrated using the PAMPA method. The results presented in this work provide useful information about designing novel anti-Alzheimer agents.

1. Introduction

The most common neurodegenerative disease and the major cause of death among the elderly population is Alzheimer's disease (AD) [1]. This multifactorial illness is characterized by various mental symptoms such as a progressive decline in cognitive function, and extensive neuronal and memory loss [2]. The pathological findings associated with AD can be exemplified by reduced acetylcholine (ACh) levels [3,4], β-amyloid (Aβ) deposits [5,6], and metal-ion imbalance [7] just to name a few [8-11]. Studies had revealed that the increased levels of ACh upon inhibition of acetylcholinesterase (AChE) improve the cognitive function and memory in AD patients [12]. Based on the cholinergic hypothesis, the leading cause of cognitive impairment in AD is attributed to the reduced levels of ACh in the brain due to the loss of cholinergic neurons [13]. Thus, the most important treatment strategy is the elevation of ACh function in CNS *via* limiting its enzymatic

Abbreviations: AD, Alzheimer's disease; ACh, Acetylcholine; AChE, Acetylcholinesterase; BChE, Butyrylcholinesterase; DTNB, (5,5-dithiobis-(2-nitrobenzoic acid)); Aβ, β-amyloid; CAS, Catalytic active site; PAS, Peripheral anionic site; MTT, (3-(4,5-dimethylthiazol-2-yl)-2,5-diphenyltetrazolium bromide); NFT, Neurofibrillary tangle; PHF, Paired helical filaments; MAP, Microtubule associated protein; ThT, Thioflavin T; HFIP, Hexafluoroisopropanol; PDB, Protein data bank; DMSO, Dimethyl sulfoxide; SI, Selectivity index; BBB, Blood-brain barrier; PAMPA, Parallel artificial membrane permeability assay

* Corresponding author at: Department of Medicinal Chemistry, School of Pharmacy, Tabriz University of Medical Sciences, Tabriz, Iran.
E-mail address: dastmalchi.s@tbzmed.ac.ir (S. Dastmalchi).

https://doi.org/10.1016/j.bioorg.2020.104186
Received 29 February 2020; Received in revised form 15 July 2020; Accepted 12 August 2020
Available online 26 August 2020

biodegradation by AChE and its evolutionary related enzyme butyrylcholinesterase (BChE) [14]. Formation of neurofibrillary tangles (NFTs) [15] composed of bundles of paired helical filaments (PHF) mainly made of the microtubule-associated protein (MAP) tau is another main cause of AD [16]. Another well-documented AD hypothesis is the aggregation and accumulation of Aβ peptide in the brain [17]. The plaques formed outside of the neural cells cause neurotoxicity and ultimately lead to cell death. Therefore, various strategies are currently explored to prevent the formation of Aβ plaques and eradicate toxic oligomers [18–20]. Numerous studies are supporting the association between AChE and Aβ aggregation into senile plaques observed in AD [21-24]. *In vitro* studies using purified or recombinant Aβ proteins showed that AChE accelerates but BChE attenuates aggregation of Aβ and formation of fibrils [25]. It has been shown that these recombinant proteins adopt different conformations and the conformer with a high β-strand secondary structure content, called amyloidogenic, is resistant to proteases and has high propensity to form Aβ aggregate. In contrast, the other conformer, i.e., non-amyloidogenic, adopted a random coil or α-helix conformation and was protease sensitive. Such behavior of Aβ peptides is used for *in vitro* evaluation of anti-Aβ aggregation activity of anti-Alzheimer drug candidates [17,26]. Co-localization of AChE with Aβ plaques in the brain provides substantial evidence for the interplay of AChE and Aβ in the pathology of AD. It is proposed that AChE binds to the Aβ non-amyloidogenic form through the peripheral site and then converts it into amyloidogenic form with the subsequent formation of amyloid fibrils [27]. The mechanism of the AChE association with amyloid plaques is not fully understood. Still, the experimental studies showed that upon the association, AChE changes its enzymatic and pharmacological properties, and prevention of such association may have beneficial effects in the treatment of AD patients [28,29]. The development of compounds capable of binding to the catalytic site of AChE, as well as its peripheral site, can be a very promising strategy [30]. The complex pathophysiology of AD, as mentioned above, requires combination therapy [31,32], and one way of getting around this is to develop multi-targeted agents, which are effective at multiple pathways simultaneously [33-36].

Proposing novel compounds capable of acting on multiple targets was investigated in the hope of developing promising agents for the treatment of AD [37]. Donepezil, a clinically used anti-AD, belongs to the class of anti-cholinesterase which contain piperidine ring. Numerous other examples exist in the literature, where piperidine containing compounds with different anti-cholinesterase potency were designed and synthesized. The range of concentration at which they inhibit cholinesterases can be quite broad from nanomolar up to a few hundred micromolar [38–41]. It was shown by both experimental and theoretical methods that the piperidine moiety of such compounds, like donepezil, is involved in π–cation interaction with the binding site of AChE [41,42]. Various studies have shown that the piperidine ring can be replaced with other groups such as pyridinium [43–45]. For example, Lan et al. have reported a series of pyridinium analogs with potent anti-cholinesterase activity [44]. Thiazoles are an important class of heterocyclic compounds with many biological effects [46–48] including anticholinesterase activity [49,50]. For example, acotiamide hydrochloride, a thiazole based selective AChEI, is in the advanced stages of clinical studies to treat functional dyspepsia [51]. Based on this observation, Sun et al. have reported a series of thiazole acetamide derivatives showing anticholinesterase activity ranging from 3.14 to 32.45 nM for a possible role in the treatment of AD [52]. Yadav and coworkers (2016) reported a series of compounds containing both piperidine and thiazole rings with the most active analog inhibiting AChE with an IC_{50} value of 0.3 μM [41]. In recent years, inspired by the structure of donepezil, some benzyl pyridinium derivatives with cholinesterase inhibitory activity were designed and synthesized [43,53,54]. The designed compounds showed potent cholinesterase inhibition.

Based on the above-mentioned evidence, it seemed reasonable to design and synthesize novel thiazole and pyridinium containing compounds as potential anticholinesterase inhibitors effective in AD. Current work reports the synthesis and cholinesterase inhibitory activities of a novel series of thiazole-pyridinium derivatives proposed using molecular hybridization-based drug design concept. The strategy was to connect the phenylthiazole segment *via* a diamide linker to benzylpyridinium moiety to provide a scaffold with two pharmacophoric groups capable of interacting with the peripheral anionic site (PAS) and catalytic active site (CAS) of AChE, respectively. The molecular hybridization design strategy used in this study was schematically shown in Fig. 1. All of the template structures used in hybridization strategy, i.e., coumarin [55], benzofuran [56,57], and benzothiazole derivatives [49,58], contain a substituted benzylpyridinium segment. Hence, in the proposed structures, the benzene ring of this segment was substituted with different functional groups with varying physico-chemical properties in terms of electronic, lipophilicity, and steric effects to provide structural diversity required to draw rational structure–activity relationship. Moreover, in the *in silico* component of the design strategy, the proposed hybrid structures were docked into the binding site of AChE and the resulting fitness scores were compared to that of donepezil as an early stage evaluation of the designed compounds. It is expected that the intrinsic dual mechanism of AChE inhibition by interacting with both CAS and PAS, and prevention of Aβ aggregation could result in the discovery of efficient anti-Alzheimer agents.

2. Results and discussion

2.1. Chemistry

To prepare compounds **7a–u** shown in Scheme 1, first, compound **3** was reacted with pyridin-4-ylmethanamine **4a** or pyridin-3-ylmethanamine **4b** in the presence of 1-ethyl-3-(3-dimethylaminopropyl) carbodiimide (EDCI) and hydroxybenzotriazole (HOBt) in dry CH_3CN at room temperature for 24 h to obtain compounds **5a** and **b**. Then, these products were reacted with appropriate benzyl halides **6** by refluxing in acetonitrile for 2–3 h to afford compounds **7a–u**. The structures of all target compounds were confirmed by IR and NMR spectroscopy, as well as MS spectrometry.

2.2. AChE and BChE inhibitory activity

In vitro inhibitory activities of the synthesized compounds **7a–u** against AChE and BChE enzymes were evaluated using Ellman's method [59] (Table 1). As reported in the table, the synthesized compounds **7a–u** can be classified into two categories based on the position of the diamide linker on the pyridinium ring. In compounds **7a–p** (series *i*), the linker is connected to *para* position, while in compounds **7q–u** (series *ii*) the linker is located in *meta* position relative to the positively charged nitrogen atom of pyridinium ring. The results illustrated in Table 1 indicate that all designed derivatives were able to inhibit AChE with IC_{50} values in the range of 0.40 to 54.58 μM. The results were compared with the inhibitory effect of donepezil (IC_{50} of 0.03 μM) used as the reference drug. The compounds demonstrated much weaker inhibitory effects (almost an order of magnitude) on BChE with the minimum IC_{50} values of 25.40 μM observed for compound **7a**. Based on the inhibitory effects on AChE and BChE, a selectivity index was calculated for those compounds demonstrating IC_{50} values less than 100 μM. The most potent AChE inhibitor was 2-fluoro compound **7d** (IC_{50} = 0.40 μM) and the second most potent inhibitor was 2-Br substituted **7j** (IC_{50} = 0.69 μM), both belonging to class *i* derivatives. In both of these most active compounds, the F and Br substituents are located in *ortho* position on the benzyl ring. Moving these functional groups in **7d** and **7j** to *meta* (**7e** and **7k**) and *para* (**7f** and **7l**) positions led to a gradual decrease in inhibitory potency. This trend of activity

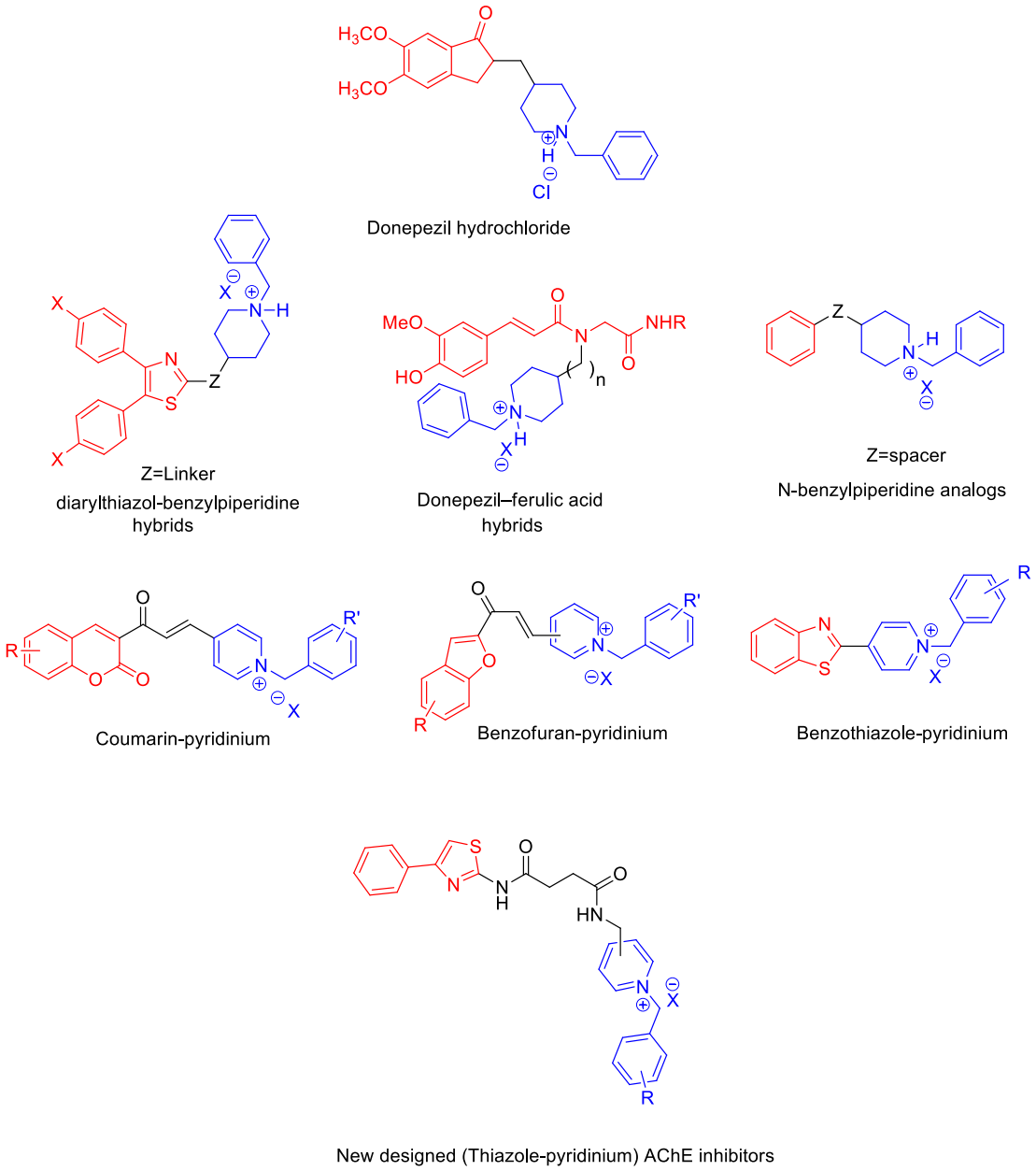

Fig. 1. The molecular hybridization strategy used for the design of novel AChE inhibitors presented in this work. The structural similarities of donepezil hydrochloride as a FDA-approved AChE inhibitor and related structures, *N*-benzylpyridinium chalconoids (derived from coumarin and benzofuran and benzothiazoles, reported as potent anti-AChE agents), and the newly designed thiazole-pyridinium AChE inhibitors were color coded in different molecules.

can also be seen for all other substitutions in series *i*. According to the results shown in Table 1, the *ortho* and *meta* substituted compounds exert stronger inhibition towards AChE than the *para* substituted derivatives (the order of substitution position is *ortho* > *meta* > *para*). As stated above, among the *ortho* substituted derivatives, 2-fluorobenzyl **7d** from class *i* showed the highest activity. The substitution of strong electron-withdrawing groups at *para* position diminished the inhibitory activities of 4-pyridinium compounds against AChE. For *para*-nitro **7c** (IC_{50} = 40.80 μM) and *para*-halogen derivatives **7f**, **7i**, and **7 l**, as the electron-withdrawing effect decreases (based on Hammett electronic constant [60], σ, supporting materials, Table S1), the activity increases. Although such a correlation between activity and electronic effect cannot be extrapolated for the methyl group, it may indicate the general pattern observed for the studied substitutions. The lipophilicity of the substituents (Hansch π constants [61], Table S1) affects the inhibitory activities of the studied compounds differently without any observable correlation. But, considering just halogen-substituted compounds, it seems that there is an inverse correlation between π values of the substituents and AChE inhibitory potency. It is known that the π lipophilicity constant may also represent other features of a substituent, such as size, and therefore the overall dissimilar pattern observed for the lipophilicity effect of the substituents in different positions may be realized. The steric feature of the substituents (evaluated by Taft's Es steric parameters, Table S1) shows overall a direct correlation to the inhibitory potency of *ortho*, *meta* and *para*-substituted derivatives, which means less steric effects leads to higher potencies [62]. The overall trend of AChE inhibition potency for the halogenated compounds is F > Cl > Br and they convey higher potency than methyl and methoxy substitutions. In general, the diversity of 3-pyridinium series (5 derivatives) is much restricted compared to the 4-pyridinium series (16 derivatives) and all of the substitutions are limited to the *para* position. The correlation observed between the physicochemical nature

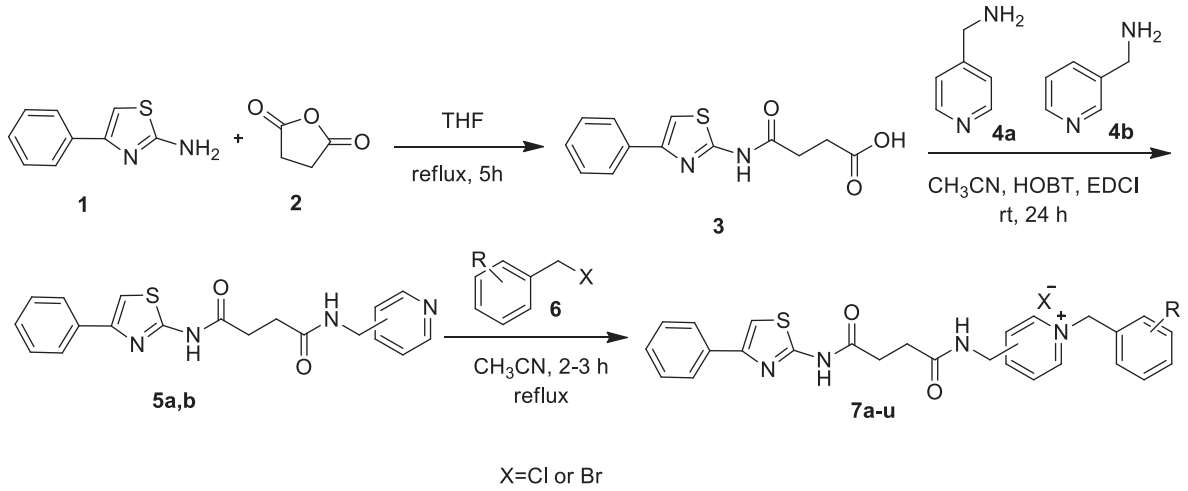

Scheme 1. General route for the synthesis of thiazole-pyridinium hybrids 7a–u.

Table 1
Cholinesterase inhibitory activity of the synthesized compounds 7a-u.

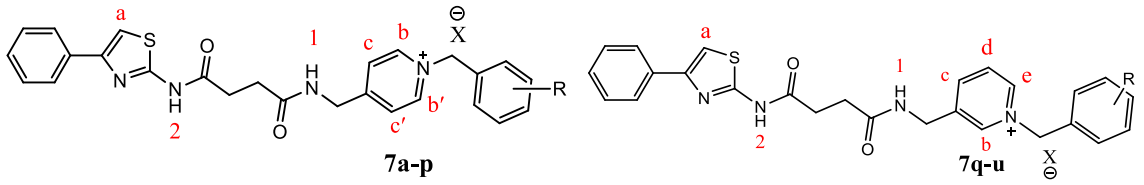

Compounds	R	X	(AChE) inhibition	(BChE) inhibition	SI
			IC_{50} μM ± SE	IC_{50} μM ± SE	
7a	H	Br	1.79 ± 0.08	25.40 ± 2.92	14.19
7b	2-NO_2	Br	14.37 ± 0.33	56.54 ± 6.51	3.93
7c	4-NO_2	Br	40.80 ± 2.82	> 100	–
7d	2-F	Cl	0.40 ± 0.04	> 100	–
7e	3-F	Br	1.29 ± 0.17	> 100	–
7f	4-F	Cl	6.48 ± 0.89	> 100	–
7g	2-Cl	Cl	0.77 ± 0.09	> 100	–
7h	3-Cl	Br	0.78 ± 0.16	> 100	–
7i	4-Cl	Cl	21.49 ± 1.98	35.29 ± 5.69	1.64
7j	2-Br	Br	0.69 ± 0.06	50.90 ± 9.38	73.77
7k	3-Br	Br	6.33 ± 0.73	> 100	–
7l	4-Br	Br	30.49 ± 7.02	> 100	–
7m	2-CH_3	Br	2.67 ± 0.24	> 100	–
7n	3-CH_3	Cl	18.24 ± 1.68	> 100	–
7o	4-CH_3	Cl	33.87 ± 3.12	> 100	–
7p	3-OCH_3	Cl	9.40 ± 1.51	> 100	–
7q	H	Br	1.64 ± 0.15	> 100	–
7r	4-NO_2	Br	54.58 ± 12.57	> 100	–
7s	4-F	Br	1.95 ± 0.27	> 100	–
7t	4-Cl	Cl	28.73 ± 6.62	> 100	–
7u	4-Br	Br	35.05 ± 8.07	88.43 ± 8.15	2.52
Donepzil			0.03 ± 0.003	5.22 ± 0.48	174

Data are expressed as Mean ± SE for three independent experiments. X is the counterion present in the final compound.
SI means Selectivity Index and is defined by $IC_{50\ (BChE)}/IC_{50\ (AChE)}$.

of the substituents in series *ii* derivatives and their AChE inhibitory potency is more or less the same as that explained above for series *i* (*para*-substituted) derivatives. Here again, the *p*-nitro compound is less potent (IC_{50} = 54.58 μM) than the halogenated derivatives, and among the different halogen groups, F grants the highest AChE inhibitory effect to compound **7s** (IC_{50} = 1.95 μM). However, the best anti-AChE activity in class *ii* compounds was shown for **7q**, unsubstituted compound (IC_{50} = 1.64 μM). Generally, in series *ii* derivatives, similar to *para*-substituted compounds in series *i*, the introduction of substitution has led to the decreased activity. This may indicate that there may be a steric hindrance associated with the substitution at the *para* position. Comparing the AChE inhibitory potency of the compounds introduced in this study with that of the previously reported inhibitors containing piperidine, pyridinium, or combined piperidine-thiazole moieties revealed that these structures may demonstrate different potencies based on their defined structure and no single structural element can promise improved activity. For instance, some piperidin containing AChE inhibitors exert stronger activity than the pyridinium based inhibitors and *vice versa* [38,39,44,63].

Table 2
Inhibitory effects of compounds 7a, 7d, 7g, 7j, 7m on Aβ self-aggregation.

Compounds	Inhibition of Aβ self-aggregation (%)[a]
7a	9.69 ± 1.76
7d	20.38 ± 1.51
7g	14.34 ± 2.04
7j	42.66 ± 1.33
7m	10.89 ± 1.18
Donepezil	14.70 ± 2.35
Curcumin	58.18 ± 0.88

[a] Inhibition of self-induced $A\beta_{1\text{-}42}$ aggregation (10 μM) produced by the tested compounds at 10 μM concentration. Values are expressed as means ± SE of three experiments.

2.3. Inhibitory effects on β-amyloid self-aggregation

The **7a** and *ortho*-substituted compounds **7d, 7g, 7j** and **7m** with potent AChE inhibitory activities were evaluated for their ability to inhibit self-aggregation of $A\beta_{1\text{-}42}$ peptide assessed by the thioflavin T (ThT) fluorescence method [64]. According to the results presented in Table 2, the most potent derivative, compound **7j,** shows (42.66% ± 1.33) inhibition of Aβ self-aggregation, three folds higher than that of donepezil (14.70 ± 2.35%). The level of inhibition of Aβ self-aggregation observed for **7j** is almost comparable to that of curcumin (58.18 ± 0.88%). The derivative **7d** was the second most potent inhibitor of Aβ fibrillization (20.38 ± 1.51%).

2.4. Evaluation of PAS binding ability of thiazole-pyridiniums

Propidium iodide (PI) is a known ligand, which binds specifically at the PAS domain of AChE, and upon binding, its fluorescence intensity increases up to eight folds [65]. The affinity of compounds **7a**, **7j** and **7m**, the most potent inhibitors of AChE, for binding to the PAS site of AChE was evaluated by PI displacement assay (Table 5). As reported in the table, compound **7j**, the most potent derivative, exhibited the most reduction in the fluorescent intensity of PI and hence possessed the highest displacement potency among the studied compounds (15.5 ± 1.1%). Taking into account that the compound **7j** also inhibits Aβ self-aggregation, one may deduce that in the presence of AChE, it can very efficiently inhibit Aβ aggregation, which in turn may have a pronounced effect on amelioration of AD. Also, molecular docking for this derivative suggested its significant interaction with PAS residues.

2.5. Neuroprotective activity of the synthesized compounds

The neuroprotective effects of compounds **7a, 7d, 7g, 7j** and **7m** against apoptosis induced in PC_{12} neuron cells by H_2O_2 were evaluated using MTT (3-(4,5-dimethylthiazol-2-yl)-2,5-diphenyltetrazolium bromide) assay (Fig. 2). The differentiated cells from PC_{12} neurons were pretreated with different concentrations (1, 10, and 100 μM) of the synthesized compounds for 3 h, before treatment with H_2O_2 (400 μM). After the addition of H_2O_2 to induce apoptosis in PC_{12} cells, the cell viability was measured by using MTT colorimetric assay. The protective effects obtained for the studied compounds at the above-stated concentrations were compared to the control group (where the cells were subjected to H_2O_2, but not incubated with any compound), and donepezil (1, 10 and 100 μM), and the results depicted in Fig. 2. Compounds **7j**, the second most active AChE inhibitor, and **7m** demonstrated reasonable neuroprotective activity akin to that seen for donepezil [66] at different studied concentrations. Compound **7d**, the most active AChE inhibitor, did not show neuroprotective activity at the used concentrations.

2.6. Evaluation of passive BBB penetration of 7j

Determination of brain permeability is one of the essential prerequisites to target the compounds for the treatment of AD. PAMPA (parallel artificial membrane permeability) assay is a technique to observe the permeability of drug molecules across the blood–brain barrier (BBB) [67,68]. This method is used to measure the effective permeability (P_e, cm/s) of the artificial lipid membrane and predict the rate of transcellular passive diffusion of test compounds through BBB. Compound **7j** with good activities in different AD-related bioassays (i.e., inhibition of Aβ self-aggregation, AChE inhibition, specific binding to PAS domain of AChE, and neuroprotective activity) was selected for PAMPA-BBB assay, and the results were compared with that of control drugs donepezil, diazepam and fexofenadine. Diazepam and fexofenadine were used as the high and low permeability standards, respectively. The equation used to determine permeability rates (P_e) is as follows:

$$P_e = C \times -ln\left(1 - \frac{[drug]_{acceptor}}{[drug]_{equilibrium}}\right), \quad \text{where} \quad C = \frac{V_D \times V_A}{(V_D + V_A) \times Area \times time}$$

V_D, V_A, Area, time, $[drug]_{acceptor}$, and $[drug]_{equilibrium}$ are the volume of donor compartment, the volume of acceptor compartment, the active surface area of membrane, incubation time (expressed in seconds), the concentration of the compound in acceptor compartment at the completion of the assay, and concentration of the compound at theoretical equilibrium, respectively.

The determined P_e value for **7j** is 5.9×10^{-6} cm/s indicating acceptable CNS penetration for this derivative. Based on the results presented in Table 6, the effective permeability of **7j** is lower than that of

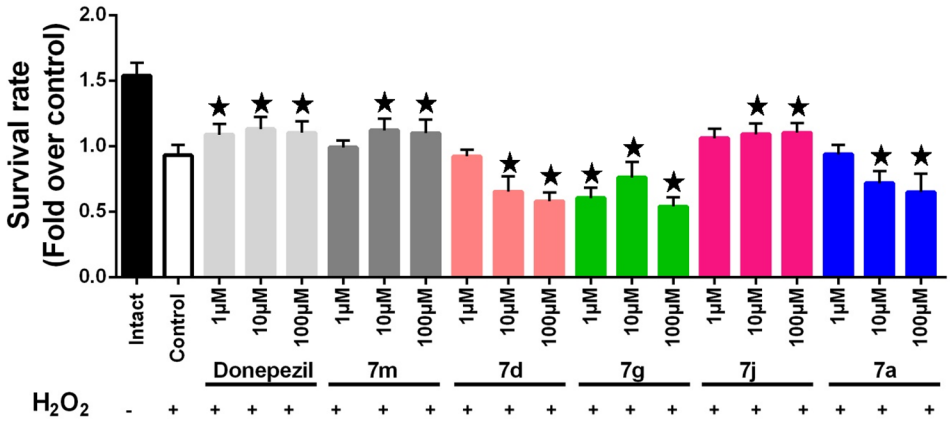

Fig. 2. Neuroprotective activity of compounds **7a**, **7d**, **7g**, **7j**, and **7m** on PC_{12} cells against H_2O_2 induced cells death. Intact cells were not exposed to either designed compounds or H_2O_2, while the control cells were treated just by H_2O_2. The cells treated with donepezil were used as positive control. The asterisk indicates statistically significant difference compared to the control group with p-value of < 0.001 based on one-way ANOVA analysis performed by Prism software.

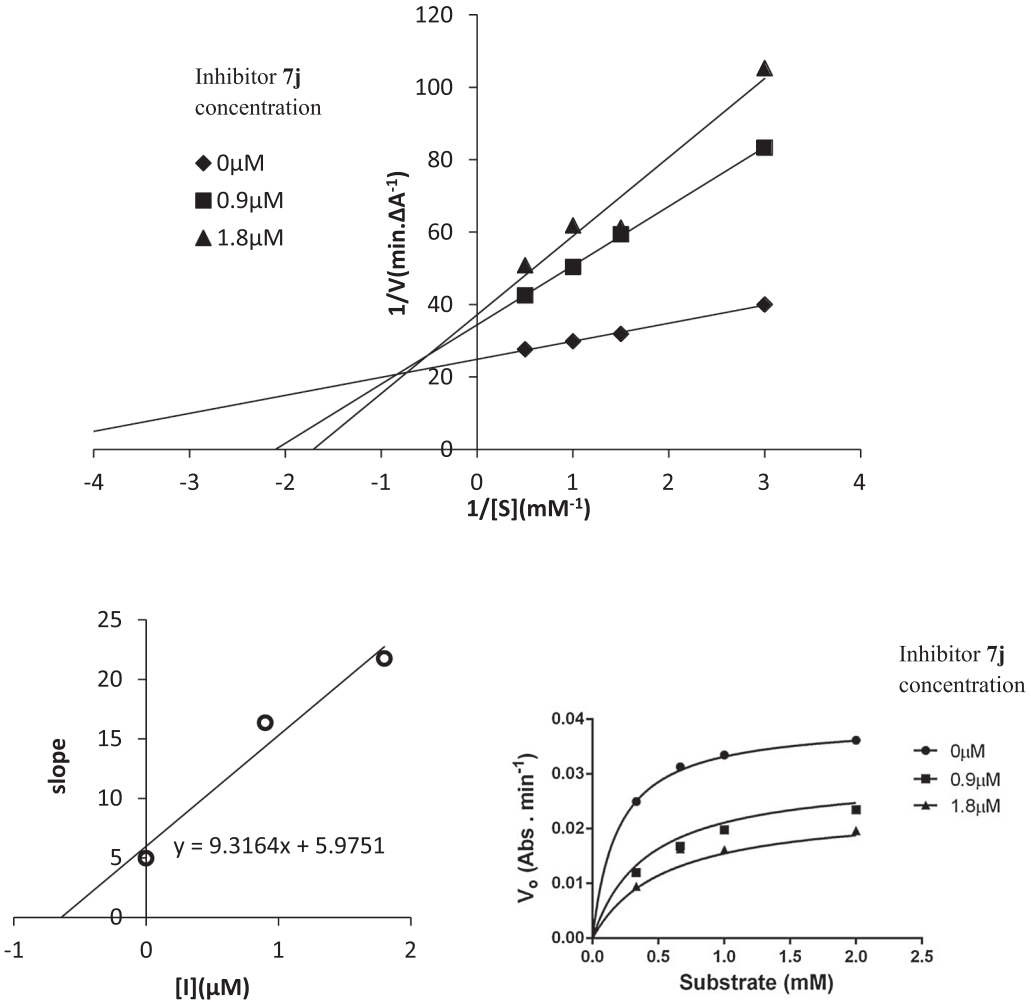

Fig. 3. Lineweavere-Burk plot, secondary plot, and enzyme kinetics profile for the inhibition of AChE by compound **7j** at 0, 0.9 and 1.8 μM concentrations to determine the inhibition mechanism as well as the steady-state inhibition constant (Ki) of the studied compound.

donepezil (7.8×10^{-6} cm/s) and diazepam (12.0×10^{-6} cm/s), which are regarded as BBB permeable drugs. However, its P_e is higher than fexofenadine (3.8×10^{-6} cm/s), an antihistamine with minor CNS side effects. According to the results, it can be deduced that **7j** may pass the BBB and exert its *in vivo* anti-AD effects.

2.7. Investigation of AChE inhibition mechanism

To reveal the mechanism by which the synthesized compounds inhibit AChE, the kinetics of inhibition was studied for the most active compounds **7d** and **7j** using Ellman's method [59]. To this end, the rate of enzyme activity in the presence of different concentrations of inhibitors ([I] equal to 0.0, 0.45, 0.9, 1.8 μM) and substrate (acetylthiocholine, [S] equal to 0.33, 0.67, 1 and 2 mM) was measured. For each inhibitor concentration [I], the initial velocity (v) was measured at different substrate concentrations [S], and the reciprocal of the initial velocity ($1/v$) was plotted against the reciprocal of the substrate concentration ($1/[S]$) to construct the Lineweaver-Burk (LWB) curve as shown in Figs. 3 and 4. The slopes and ($1/v$)-axis intercepts of the obtained lines in LWB plot were used to generate secondary plots, slope and y-intercept replots, where one can estimate the K_i and α factor (the factor by which K_s changes in the presence of inhibitor) values from the abscissa intercepts of the lines. The following equations show the bases of the LWB, slope and y-intercept plots:

$$\frac{1}{v} = \frac{K_s}{V_{max}}\left(1 + \frac{[I]}{K_i}\right)\frac{1}{[S]} + \frac{1}{V_{max}}\left(1 + \frac{[I]}{\propto K_i}\right) \quad (1)$$

$$\left(\frac{1}{v}\right) - axis \;\; intercept = \frac{1}{V_{max} \propto K_i} \times \frac{1}{[I]} + \frac{1}{V_{max}} \quad (2)$$

$$\text{Slope} = \frac{K_s}{V_{max} K_i} \times \frac{1}{[I]} + \frac{K_s}{V_{max}} \quad (3)$$

where v, V_{max}, K_s, K_i, and α are initial velocity, maximum enzyme velocity without inhibitor, enzyme-substrate dissociation constant, enzyme-inhibitor dissociation constant, and α factor.

The data were also analyzed using the nonlinear regression method implemented in GraphPad Prism program (version 6.01, GraphPad Inc, 2012). The obtained LWB plot represented a non-competitive mixed-type inhibition pattern for both compounds **7d** and **7j**. In non-competitive inhibition, the lines in the LWB plot intersect the horizontal axis. However, the intersection point may also lie above or below the axis [69]. In such cases, which happen most of the time, the inhibition is called mixed-type inhibition. A non-competitive inhibitor binds to both free enzyme and enzyme-substrate complex affecting both the slope and the vertical intercept of a Lineweaver–Burk plot [69,70]. The K_i values calculated using the secondary plots and nonlinear method were 0.79 μM and 0.77 μM for **7d** and 0.64 μM and 0.50 μM for **7j**, respectively (Figs. 3 and 4). The kinetic parameters of AChE inhibition by **7d** and **7j** are shown in Table 3.

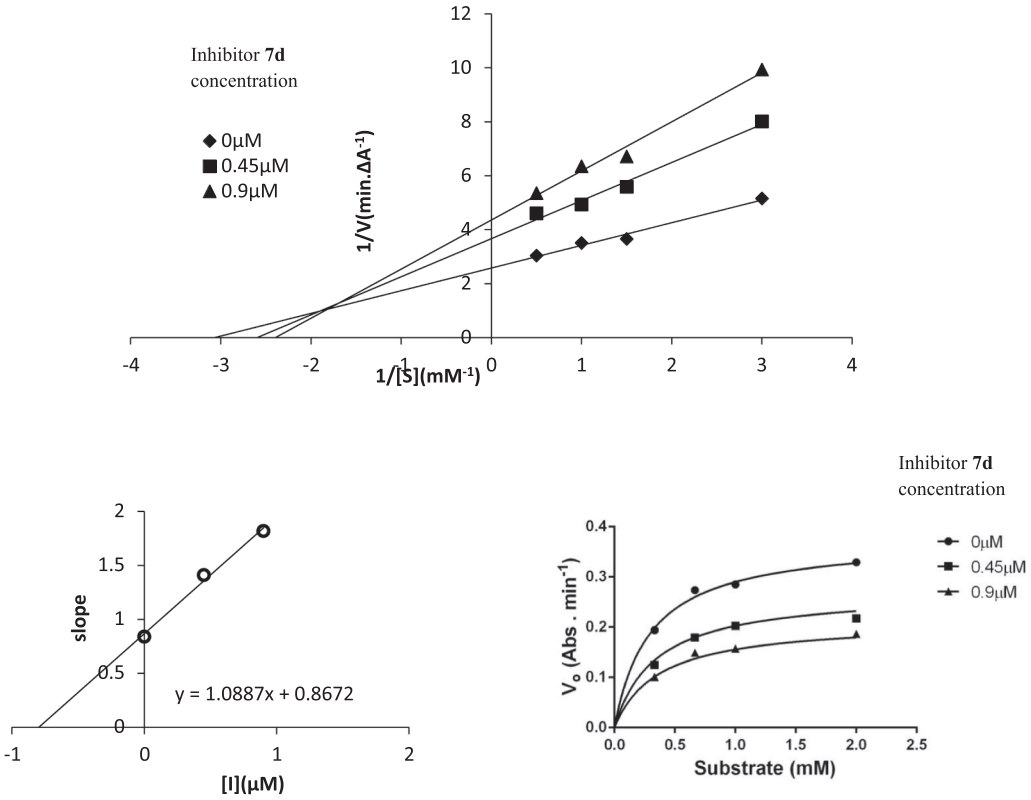

Fig. 4. Lineweavere-Burk plot, secondary plot, and enzyme kinetics profile for the inhibition of AChE by compound **7d** (the inhibitor) at 0, 0.45 and 0.9 μM concentrations to determine the inhibition mechanism as well as the steady-state inhibition constant (Ki) of studied compound.

Table 3
The kinetic parameters of AChE inhibition by 7d and 7j.

Compounds	V_{max} Abs min^{-1}	K_m mM	K_i μM	α
7d	0.390 (0.380)	0.32 (0.29)	0.79 (0.77)	1.7 (1.5)
7j	0.040 (0.039)	0.20 (0.19)	0.64 (0.50)	5.9 (5.6)

The values in the **parentheses** are from Prism GraphPad calculation.

2.8. Docking studies

At the initial stages of the study, docking calculations were used to evaluate the binding of the designed compounds to AChE. First, it was noted that the best docking condition (scoring function and genetic algorithm (GA) search parameters) to reproduce the experimentally observed binding pose of donepezil could be achieved using the ASP scoring function as outlined in the experimental section. Then, the same docking strategy was applied for the docking of designed compounds, and the results were compared to that of donepezil. The docking fitness scores for the designed compounds ranged from 65 to 73. Comparing these scores to that calculated for donepezil (i.e., ~70) indicated that the proposed compounds may show AChE inhibition potency close to that of donepezil, and some may even have higher potencies. With this initial *in silico* assessment on the binding, the synthesis and biological evaluation of the designed compounds were carried out as outlined in the previous sections. At each step, more promising compounds have been selected for further investigations in the next steps. In this way, two most promising derivatives **7j** and **7d** were selected to investigate their AChE inhibition mechanisms and more detailed docking studies. There are many experimental structures available for AChE from different sources in the protein data bank (PDB). The enzyme inhibition potency of the synthesized derivatives in this study was determined using eel AChE. Therefore, it seems more appropriate to do the docking of the derivatives using the structure of the same enzyme. Due to (*i*) the low resolution of experimental structures (PDB codes: 1C2O, 1C2B, 1EEA) for eel AChE [71] and much higher resolution of hAChE structure (4EY7) in PDB, (*ii*) minor differences between human and eel AChE structures, (*iii*) lack of difference between residues forming the binding site of human and eel AChEs, and (*iv*) presence of a ligand (donepezil) in the binding site of hAChE structure, [42,72] it seemed appropriate to perform the docking calculations of the selected compounds using experimental hAChE structure. To optimize the parameters for the docking experiments, first donepezil structure present in 4EY7 was removed, and then a new structural file for donepezil was prepared and energy optimized, and subsequently was used for the docking calculation using the GOLD program. The residues within the 6 Å from the co-crystallized donepezil were defined as the active residues in the binding site. Furthermore, three water molecules present in the binding pocket of the experimental structure and known to be involved in hydrogen-bonds with donepezil and the enzyme were retained. Different scoring functions available in the GOLD program were used, and then the RMSD value between the experimental and docked donepezil was calculated. The minimum RMSD (0.55 Å) was obtained using ASP [73] scoring function. All experimentally observed interactions for donepezil-AChE complex (4EY7 structure) were present in the complex obtained by docking calculations (see. Fig. S1 of the supporting materials). Using the same parameter set identified for the optimum docking of donepezil, compounds **7j** and **7d** were docked in the binding site of human AChEs experimental structure (4EY7). The modes of interaction for the most promising compounds **7d** and **7j** were discussed below for the docking calculations performed using 4EY7 structure.

The results of docking calculations indicated a high similarity between the interactions seen for the most potent compounds **7d** and **7j**. Fig. 5 shows the docking pose for compound **7d**. The more detailed visual illustrations of the interactions revealed by docking results for this compound are shown in Fig. 6, panels A, B, and C. According to the results, in compound **7d**, benzyl moiety plays a vital role in ligand recognition via π-π stacking interaction with Trp^{86} residue. In addition,

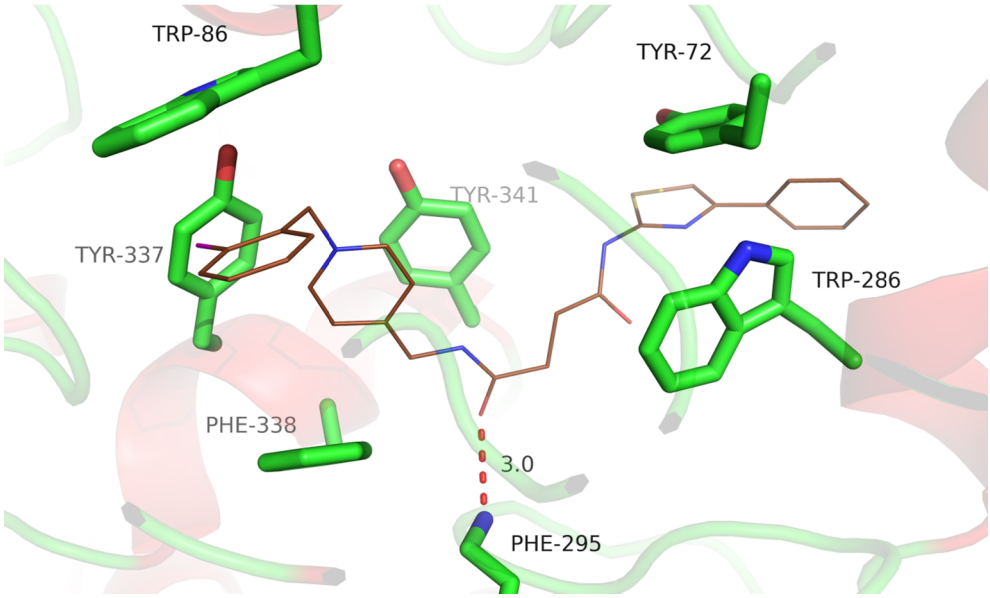

Fig. 5. Three-dimensional illustration of **7d** docked into the binding site of human AChE. The enzyme is depicted in transparent carton representation while the residues interacting with **7d** are shown in stick mode. Compound **7d** is shown in line representation for clarity. Distance between heavy atoms for H-bind observed between amid nitrogen atom of Phe[295] and oxygen atom of amide group proximal to pyridinium ring in **7d** is illustrated by dashed red line. The image was generated using PyMol (Version 1.5.X, Open-Source PyMol, Schrodinger, LLC). (For interpretation of the references to color in this figure legend, the reader is referred to the web version of this article.)

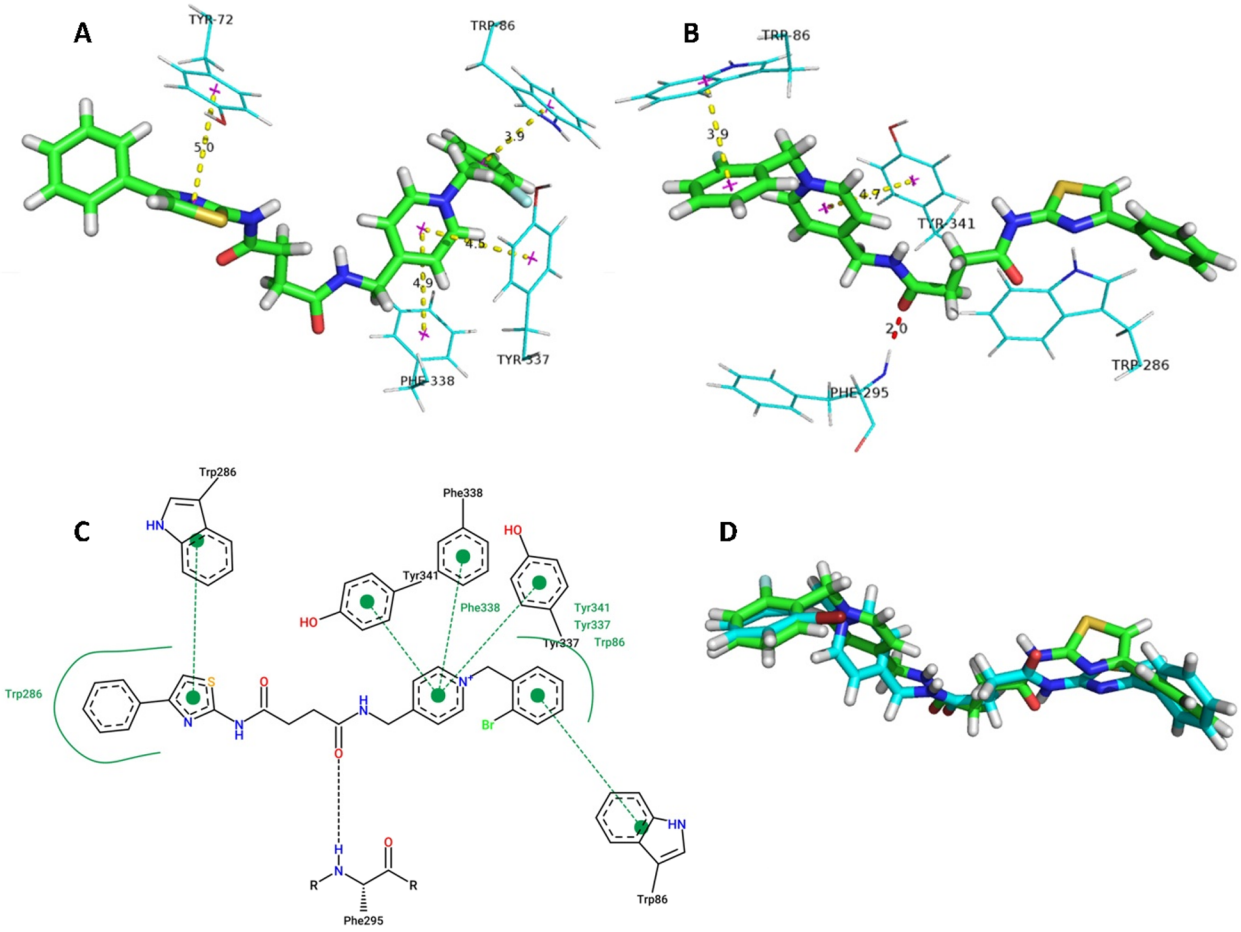

Fig. 6. Three- and two-dimensional illustrations of the binding of compound **7d** with human AChE. Three dimensional representations of the residues interacting with **7d** are shown in panels A and B from two different angles for more clarity. Hydrogen-bond and π-π/π-cation interactions are shown by red and yellow dotted lines. The images were generated using PyMol (Version 1.5.X, Open-Source PyMol, Schrodinger, LLC). Panel C shows 2D representation of the key interactions between **7d** docked into the binding site of human AChE prepared using PoseView program. The residues involved in hydrophobic interactions are shown in green and the corresponding areas in **7d** are indicated by green curved lines. The side chain of residues form AChE and the corresponding functional group in **7d** involved in π-π/π-cation interactions are indicated by green dots linked by green dotted lines. H-bond interaction was indicated by black dotted line. Panel D shows the relative positions of **7d** (green) and **7j** (cyan), the two most potent derivatives, while docked into the binding site of human AChE. (For interpretation of the references to color in this figure legend, the reader is referred to the web version of this article.)

pyridinium moiety interacts with Tyr^{337}, Phe^{338}, and Tyr^{341}, via π-π stacking/π-cation interactions. Furthermore, the thiazole ring also interacts with Tyr^{72} via π-π stacking interaction. There is a hydrogen bonding interaction formed between the oxygen atom of the carbonyl group proximal to the pyridinium ring of **7d** with amide hydrogen of Phe^{295} residue. Trp^{86}, Trp^{286}, Tyr^{337}, and Tyr^{341} residues stabilize **7d** in the binding pocked through hydrophobic interactions. Docking-based identified interactions between **7d** and AChE are mostly in common with those reported experimentally for donepezil (i.e., shown in crystal structure 4EY7). Donepezil shows π-π stacking with Trp^{86} and Trp^{286}, H-bonding with Phe^{295}, and hydrophobic interactions with Trp^{86}, Trp^{286}, Tyr^{337}, Phe^{338} and Tyr^{341}. The identified commonalities between the mode of interactions observed for compound **7d** and donepezil may indicate similar AChE inhibition mechanism by this series of compounds. Compound **7j**, the other most potent derivative, illustrates very close modes of interactions with hAChE predicted by docking calculations. The binding mode involves π-π stacking interaction between thiazole and indol side chain of Trp^{286}, π-cation interactions between quaternary nitrogen of pyridinium ring with Tyr^{337} Phe^{338}, and Tyr^{341} residues, and hydrophobic interactions with Trp^{86}, Trp^{286}, Tyr^{337}, Phe^{338}, and Tyr^{341} residues. Also, the benzyl moiety interacts with Trp^{86} residue via π-π stacking interaction. Furthermore, a hydrogen bonding interaction was observed between the oxygen atom of the carbonyl group of compound **7j** close to pyridinium ring with the backbone amide hydrogen of Phe^{295} residue similar to that seen for compounds **7d** and donepezil. Fig. 6 (panel D) shows the relative position of **7d** and **7j** compounds while docked into the binding site of human AChE. As can be seen in the figure, the corresponding molecular moieties in two compounds are positioned very close to each other and therefore making similar interactions with the enzyme. In agreement with the results of kinetic studies, docking investigation confirmed the mixed-type of AChE inhibition mechanism for compounds **7d** and **7j** due to their interaction with both CAS and PAS sites of the enzyme as described above. Such an inhibition mechanism was also shown for donepezil and other donepezil like derivatives. The experimental and *in silico* structural studies revealed that donepezil and similar compounds occupy both CAS and PAS binding sites of AChE [42,43,74], which are in accordance with their mixed-type non-competitive inhibition mechanisms proposed based on analyzing the kinetics of enzyme inhibition using LWB and other methods [54]. In contrast to mixed-type inhibitors, pure non-competitive inhibitors only bind to allosteric PAS site of the enzyme and lines in the LWB plot intersect on the x-axis (i.e., $1/S$ axis). For example, it was shown that bromotyrosine-derived alkaloids inhibit AChE in a non-competitive manner deduced from the LWB and docking analyses [75]. On the other hand, in the presence of competitive inhibitors, the V_{max} of enzymatic reaction does not change, but the apparent K_m value increases leading to a LWB plot where the lines intersect on the y-axis ($1/v$ axis). For example, using docking studies and enzyme kinetic assay, Rizvi et al. showed that glimepiride interacts with the substrate binding site of AChE (i. e., CAS) and in the obtained LWB plot, lines intersect on the y-axis indicating a pure competitive inhibition [76]. In summary, based on the results of docking calculations and kinetic studies of AChE inhibition by compounds **7d** and **7j** a mixed non-competitive inhibition mechanism is proposed for the studied compounds.

2.9. Prediction of physicochemical properties

Some physicochemical properties related to the drug-likeness of compounds **7d** and **7j** including octanol/water partition coefficients (Clog P), number of H-bond acceptors (HBA), number of H-bond donors (HBD), polar surface area (tPSA), and number of rotatable bonds (RBC) were calculated and shown in Table 4. Based on the results, these compounds pass the drug-likeness rules proposed by Lipinski [77], Egan [78], and Muegge [79], while violating one or two criteria in other drug-likeness systems. For example, the number of rotatable bonds (RBC) for **7d** and **7j** exceed maximum acceptable numbers defined by Ghose [80] and Veber [81]. Collectively, it is anticipated that **7d** and **7j** may show reasonable ADMET properties, but is yet to be determined experimentally.

Table 4
Physicochemical properties for the compounds 7d and 7j.

Compounds	MW	C logP	HBA	HBD	tPSA	RBC
7d	475.5	−1.23 ± 0.60	4	2	103.21	11
7j	536.4	−0.51 ± 0.60	3	2	103.21	11

Clog P: Calculated *n*-octanol–water partition coefficient, HBA: H-bond acceptors, HBD: H-bond donors, tPSA: topological polar surface area, RBC: Rotatable bond count.

Table 5
The results of propidium iodide displacement assay for compounds **7a**, **7j** and**7m**.

Compounds	Propidium iodide displacement from PAS-AChE (% inhibition)
7a	11.6 ± 1.5
7j	15.5 ± 1.1
7m	5.3 ± 0.8
Donepezil	20.2 ± 1.3

Values are reported as mean ± SEM for three independent experiments. Propidium iodide displacement assay was performed on AChE to test the ability of compounds to displace propidium from PAS-AChE. Donepezil, an anti-AD drug with known PAS binding property, was used as positive control.

Table 6
The results of PAMPA-BBB assay for compound **7j** and Donepezil, Diazepam and Fexofenadine were used as controls.

Compounds	PAMPA-BBB permeability P_e (10^{-6}cm.s^{-1})
7j	5.9 ± 0.1
Donepezil	7.8 ± 0.3
Diazepam	12.0 ± 1.5
Fexofenadine	3.8 ± 0.3

All the results are expressed as means ± SE of three experiments.

3. Conclusion

Cholinesterase inhibitors play a crucial role in cholinergic signaling, and hence, they are regarded as the first-line therapeutics in alleviating the symptoms of Alzheimer's disease. Such inhibitors, exemplified by donepezil, can also slow down the amyloidogenic product formation, apart from increasing the levels of ACh. In the current study, a novel series of thiazole-pyridinium hybrids were synthesized, and evaluated against AChE and BChE using Ellman's method. Results showed that all derivatives were selective for AChE, and among them, compounds **7d** and **7j** demonstrated the highest AChE inhibitory effects with IC_{50} values of 0.40 and 0.69 μM, respectively. In addition, **7j** was three times more potent than donepezil, the reference drug, in preventing Aβ aggregation. Based on docking studies, it was proposed that compounds **7d** and **7j** form key interactions with both CAS and PAS regions of AChE. The specific interaction with the latter site was evaluated using the PAS site marker displacement technique further confirming the ability of these derivatives acting as Aβ aggregation inhibitors. Furthermore, compound **7j** showed very good neuroprotective activity against H_2O_2 induced oxidative stress. The results of *in vitro* PAMPA assay showed that **7j** is capable of passing BBB and exerting its anti-AD effects. Collectively, although the more promising derivatives show less AChE inhibitory potency than the standard drug donepezil, however, they are better inhibitors of Aβ aggregation while exerting similar

neuroprotective activity. The results obtained in this work showed that the thiazole-pyridinium structure may represent a new useful multi-targeted scaffold for the development of novel anti-Alzheimer agents.

4. Experimental section

4.1. Chemistry

All of the melting points were measured using Kofler hot stage apparatus. For all derivatives, ^{1}H and ^{13}C nuclear magnetic resonance (NMR) spectra were obtained on a Bruker FT-500 spectrometer, using TMS as an internal standard. The IR spectra were recorded by Nicolet Magna FTIR 550 spectrophotometer using KBr disk sample preparation method. Mass spectra were acquired on Agilent 6410 triple quadrupole liquid chromatography-mass spectrometer equipped with an electrospray ionization (+ESI) system. The purity of the compounds was assessed by HPTLC analysis. All reagents were purchased from Sigma Aldrich, Merck and Fluka unless otherwise stated.

4.2. The general procedure for the synthesis of thiazole-pyridinium hybrids *7a–u*

To the solution of compound **3** (1 mmol) in dry acetonitrile (10 mL) was added EDCI (1 mmol) and HOBt (1 mmol) and the mixture was stirred at room temperature (RT) for 30 min. Then, the mixture was added pyridin-4-ylmethanamine **4a** (or pyridin-3-ylmethanamine **4b**) (1 mmol) and the reaction was continued at room temperature for 24 h. After completion of reaction, the solvent was reduced under vacuum and the residue was dissolved in dichloromethane and washed with sodium carbonate (10%). The organic phase was dried using Na_2SO_4 and evaporated under vacuumed condition at RT. Finally, to 10 mL of dry acetonitril were added compound **5a** or **5b** (1 mmol) and appropriate benzyl halides **6** (1.2 mmol) and the reaction mixture was refluxed for 2–3 h. After completion of the reaction assessed by TLC, the solid product **7** was collected by filtration and purified using recrystallization in ethanol-petroleum ether mixture.

4.2.1. 1-Benzyl-4-((4-oxo-4-((4-phenylthiazol-2-yl)amino)butanamido) methyl)pyridin-1-ium bromide (*7a*)

Yield: 85%; mp: 232–234 °C; IR (KBr) (ν_{max}/cm^{-1}): 3197 and 3046 (2NH), 1672 and 1639 (2C═O). ^{1}H NMR(DMSO-d_6, 500 MHz): δ (ppm) = 2.60 and 2.74 (t, J = 6.7 Hz, 4H, CH_2—CH_2), 4.54 (d, J = 5.8 Hz, 2H, CH_2—NH), 5.79 (s, 2H, $-CH_2N^+$), 7.33 (t, J = 7.5 Hz, 1H, H aromatic), 7.39–7.45 (m, 5H, H aromatic), 7.50 (d, J = 6.5 Hz, 2H, H aromatic), 7.61 (s, 1H, H_a thiazole), 7.90 (d, J = 7.5 Hz, 2H, H aromatic), 8.00 (d, J = 6.5 Hz, 2H, H_c,$H_{c'}$ pyridine), 8.78 (t, J = 5.8 Hz, 1H, N—H_1), 9.09 (d, J = 6.5 Hz, 2H, H_b,$H_{b'}$ pyridine), 12.29 (s, 1H, N—H_2). ^{13}C NMR (DMSO-d_6, 125 MHz): δ (ppm) = 29.4, 30.0, 41.6, 62.5, 107.9, 125.7, 125.8, 127.7, 128.6, 128.9, 129.1, 129.5, 134.2, 134.3, 144.1, 148.7, 157.8, 160.3, 170.8 and 171.9 (2C═O). MS (*m/z*, %): 457.3 (M+, 100). Purity: > 99%.

4.2.2. 1-(2-Nitrobenzyl)-4-((4-oxo-4-((4-phenylthiazol-2-yl)amino) butanamido)methyl) pyridin-1-ium bromide (*7b*)

Yield: 70%; mp: 224–226 °C; IR (KBr) (ν_{max}/cm^{-1}): 3189 and 3058(2NH), 1688 and 1654 (2C═O). ^{1}H NMR(DMSO-d_6, 500 MHz): δ (ppm) = 2.63 and 2.77 (t, J = 6.7 Hz, 4H, CH_2—CH_2), 4.60 (d, J = 5.7 Hz, 2H, CH_2—NH), 6.17 (s, 2H, $-CH_2N^+$), 7.15 (d, J = 8.0 Hz, 1H, H aromatic), 7.32 (t, J = 7.5 Hz, 1H, H aromatic), 7.43 (t, J = 7.5 Hz, 2H, H aromatic), 7.57 (s, 1H, H_a thiazole,), 7.73 (t, J = 8.0 Hz, 1H, H aromatic), 7.80 (t, J = 8.0 Hz, 1H, H aromatic), 7.89 (d, J = 7.5 Hz, 2H, H aromatic), 8.06 (d, J = 6.5 Hz, 2H, H_c,$H_{c'}$ pyridine), 8.26 (d, J = 8.0 Hz, 1H, H aromatic), 8.83 (t, J = 5.8 Hz, 1H, N—H_1), 8.98 (d, J = 6.5 Hz, 2H, H_b,$H_{b'}$ pyridine), 12.31 (s, 1H, N—H_2). ^{13}C NMR (DMSO-d_6, 125 MHz): δ (ppm) = 29.6, 30.2, 41.7, 59.9, 107.8, 125.6, 127.7, 128.3, 128.7, 129.0, 130.5, 130.6, 131.5, 134.2, 134.9, 144.8, 147.6, 148.7, 157.8, 160.9, 170.9 and 172.1 (2C═O). MS (*m/z*, %): 502.3 (M^+, 100). Purity: 90%.

4.2.3. 1-(4-Nitrobenzyl)-4-((4-oxo-4-((4-phenylthiazol-2-yl)amino) butanamido)methyl) pyridin-1-ium bromide (*7c*)

Yield: 72%; mp: 214–216 °C; IR (KBr) (ν_{max}/cm^{-1}): 3232 and 3046 (2NH), 1670 and 1605 (2C═O). ^{1}H NMR(DMSO-d_6, 500 MHz) :δ (ppm) = 2.61 and 2.75 (t, J = 6.7 Hz, 4H, CH_2—CH_2), 4.56 (d, J = 5.7 Hz, 2H, CH_2—NH), 5.98 (s, 2H, $-CH_2N^+$), 7.32–7.42 (m, 3H, H aromatic), 7.58 (s, 1H, H_a thiazole), 7.76 (d, J = 8.0 Hz, 2H, H aromatic), 7.88 (d, J = 7.5 Hz, 2H, H aromatic), 8.04 (d, J = 6.5 Hz, 2H, H_c,$H_{c'}$ pyridine), 8.26 (d, J = 8 Hz, 2H, H aromatic), 8.80 (t, J = 5.8 Hz, 1H, N—H_1), 9.14 (d, J = 6.5 Hz, 2H, H_b,$H_{b'}$ pyridine), 12.26 (s, 1H, N—H_2). ^{13}C NMR (DMSO-d_6, 125 MHz): δ (ppm) = 29.4, 30.0, 41.7, 61.4, 107.8, 124.2, 125.8, 126.0, 127.7, 128.6, 129.9, 134.2, 141.2, 144.5, 147.8, 148.7, 158.0, 160.8, 170.9 and 172.0 (2C═O). MS (*m/z*, %): 502.3 (M^+, 100). Purity: 97%.

4.2.4. 1-(2-Fluorobenzyl)-4-((4-oxo-4-((4-phenylthiazol-2-yl)amino) butanamido)methyl) pyridin-1-ium chloride (*7d*)

Yield: 80%; mp: 196–198 °C; IR (KBr) (ν_{max}/cm^{-1}): 3332 and 3171 (2NH), 1673 and 1604 (2C═O). ^{1}H NMR(DMSO-d_6, 500 MHz): δ (ppm) = 2.57 and 2.74 (t, J = 6.7 Hz, 4H, CH_2—CH_2), 4.55 (d, J = 5.7 Hz, 2H, CH_2—NH), 5.91 (s, 2H, $-CH_2N^+$), 7.25 (d, J = 5.6 Hz, 1H, H aromatic), 7.30–7.44 (m, 5H, H aromatic), 7.59–7.61 (m, 2H, H_a thiazole, H aromatic), 7.90 (d, J = 7.3 Hz, 2H, H aromatic), 8.01 (d, J = 6.5 Hz, 2H, H_c,$H_{c'}$ pyridine), 8.57 (t, J = 5.8 Hz, 1H, N—H_1), 9.03 (d, J = 6.5 Hz, 2H, H_b,$H_{b'}$ pyridine), 12.28 (s, 1H, N—H_2). ^{13}C NMR (DMSO-d_6, 125 MHz): δ (ppm) = 29.7, 30.2, 41.7, 61.6, 107.8, 116.2 ($J_{C–F}$ = 20.0 Hz), 121.9, 125.6, 125.7, 127.7, 128.7, 129.3, 131.8, 131.9 134.3, 144.8, 148.6, 157.9, 160.7, 162.2 ($J_{C–F}$ = 249.7 Hz), 170.9, 171.4 (2C═O). MS (*m/z*, %): 475.3 (M^+, 100). Purity: > 99%.

4.2.5. 1-(3-Fluorobenzyl)-4-((4-oxo-4-((4-phenylthiazol-2-yl)amino) butanamido)methyl) pyridin-1-ium bromide (*7e*)

Yield: 80%; mp: 226–228 °C; IR (KBr) (ν_{max}/cm^{-1}): 3196 and 3042(2NH), 1672 and 1639 (2C═) ^{1}H NMR (DMSO-d_6, 500 MHz): δ (ppm) = 2.61 and 2.75 (t, J = 6.7 Hz, 4H, CH_2—CH_2), 4.55 (d, J = 5.7 Hz, 2H, CH_2—NH), 5.81 (s, 2H, $-CH_2N^+$), 7.25 (t, J = 8.0 Hz, 1H, H aromatic) 7.31–7.49 (m, 6H, H aromatic), 7.60 (s, 1H, H_a thiazole), 7.90 (d, J = 7.5 Hz, 2H, H aromatic), 8.02 (d, J = 6.5 Hz, 2H, H_c,$H_{c'}$ pyridine), 8.79 (t, J = 5.8 Hz, 1H, N—H_1), 9.11 (d, J = 6.5 Hz, 2H, H_b,$H_{b'}$ pyridine), 12.30 (s, 1H, N—H_2). ^{13}C NMR (DMSO-d_6, 125 MHz): δ (ppm) = 29.4, 30.0, 41.6, 61.8, 107.7, 115.8 ($J_{C–F}$ = 22.4 Hz), 116.2 ($J_{C–F}$ = 20.7 Hz), 124.9, 125.6, 127.7, 128.7, 131.3, 131.4, 134.3, 136.7, 144.1, 148.7, 157.8, 160.5, 162.1 ($J_{C–F}$ = 243.8 Hz), 170.9, 172.0 (2C═O). MS (*m/z*, %): 475.3 (M^+, 100). Purity: 96%.

4.2.6. 1-(4-Fluorobenzyl)-4-((4-oxo-4-((4-phenylthiazol-2-yl)amino) butanamido)methyl) pyridin-1-ium chloride (*7f*)

Yield: 85%; mp: 188–190 °C; IR (KBr) (ν_{max}/cm^{-1}): 3333 and 3183(2NH), 1674 and 1603 (2C═O). ^{1}H NMR(DMSO-d_6, 500 MHz): δ (ppm) = 2.57 and 2.74 (t, J = 6.7 Hz, 4H, CH_2—CH_2), 4.54 (d, J = 5.7 Hz, 2H, CH_2—NH), 5.78 (s, 2H, $-CH_2N^+$), 7.25–7.33 (m, 3H, H aromatic), 7.42 (t, J = 7.5 Hz, 2H, H aromatic), 7.60–7.62 (m, 3H, H_a thiazole, H aromatic), 7.89 (d, J = 7.5 Hz, 2H, H aromatic), 7.99 (d, J = 6.5 Hz, 2H, H_c,$H_{c'}$ pyridine), 8.57 (t, J = 6 Hz, 1H, N—H_1), 9.09 (d, J = 6.5 Hz, 2H, H_b,$H_{b'}$ pyridine), 12.28 (s, 1H, N—H_2). ^{13}C NMR (DMSO-d_6, 125 MHz): δ (ppm) = 29.4, 30.0, 41.0, 61.7, 107.8, 116.2 ($J_{C–F}$ = 21.1 Hz), 122.0, 125.6, 127.7, 128.7, 131.4, 131.6, 134.3, 144.6, 148.7, 157.9, 160.2, 162.2 ($J_{C–F}$ = 251.3 Hz), 170.9, 171.4 (2C═O). MS (*m/z*, %): 475.3 (M^+, 100). Purity: > 99%.

*4.2.7. 1-(2-Chlorobenzyl)-4-((4-oxo-4-((4-phenylthiazol-2-yl)amino) butanamido)methyl) pyridin-1-ium chloride (**7g**)*

Yield: 80%; mp: 190–192 °C; IR (KBr) (ν_{max}/cm^{-1}): 3333 and 3170 (2NH), 1673 and 1603 (2C═O). ^{1}H NMR(DMSO-d_6, 500 MHz) :δ (ppm) = 2.56 and 2.74 (t, J = 6.9 Hz, 4H, CH_2—CH_2), 4.58 (d, J = 5.9 Hz, 2H, CH_2—NH), 5.94 (s, 2H, —CH_2N^+), 7.25 (d, J = 5.7 Hz, 1H, H aromatic), 7.30–7.44 (m, 5H, H aromatic), 7.59–7.61 (m, 2H, H_a thiazole, H aromatic), 7.90 (d, J = 7.1 Hz, 2H, H aromatic), 8.03 (d, J = 6.5 Hz, 2H, H_c,$H_{c'}$ pyridine), 8.57 (t, J = 6 Hz, 1H, N—H_1), 9.0 (d, J = 6.5 Hz, 2H, H_b,$H_{b'}$ pyridine), 12.28 (s, 1H, N—H_2). ^{13}C NMR (DMSO-d_6, 125 MHz): δ (ppm) = 29.4, 30.0, 41.0, 61.0, 107.8, 122.0, 125.6, 127.7, 128.1, 128.7, 129.3, 130.1, 131.4, 131.6, 133.8, 134.3, 144.6, 148.7, 157.9, 160.9, 170.9, 171.3 (2C═O). MS (*m/z*, %): 491.2 (M^+, 100). Purity: 97%.

*4.2.8. 1-(3-Chlorobenzyl)-4-((4-oxo-4-((4-phenylthiazol-2-yl)amino) butanamido)methyl) pyridin-1-ium bromide (**7h**)*

Yield: 82%; mp: 225–227 °C; IR (KBr) (ν_{max}/cm^{-1}): 3194 and 3065(2NH), 1672 and 1640 (2C═O). ^{1}H NMR(DMSO-d_6, 500 MHz): δ (ppm) = 2.61 and 2.75 (t, J = 6.5 Hz, 4H, CH_2—CH_2), 4.55 (d, J = 5.7 Hz, 2H, CH_2—NH), 5.82 (s, 2H, —CH_2N^+), 7.33 (t, J = 7.0 Hz, 1H, H aromatic) 7.41–7.50 (m, 5H, H aromatic), 7.59 (s, 1H, H_a thiazole), 7.69 (s, 1H, H aromatic), 7.90 (d, J = 7.5 Hz, 2H, H aromatic), 8.02 (d, J = 6.5 Hz, 2H, H_c,$H_{c'}$ pyridine), 8.78 (t, J = 5.8 Hz, 1H, N—H_1), 9.13 (d, J = 6.5 Hz, 2H, H_b,$H_{b'}$ pyridine), 12.27 (s, 1H, N—H_2). ^{13}C NMR (DMSO-d_6, 125 MHz): δ (ppm) = 29.4, 30.0, 41.6, 61.7, 107.8, 125.7, 125.9, 127.7, 128.7, 128.9, 129.4, 129.6, 131.1, 133.6, 134.2, 136.5, 144.2, 148.7, 157.8, 160.5, 170.9, 172.0 (2C═O). MS (*m/z*, %): 491.2 (M^+, 100). Purity: > 99%.

*4.2.9. 1-(4-Chlorobenzyl)-4-((4-oxo-4-((4-phenylthiazol-2-yl)amino) butanamido)methyl) pyridin-1-ium chloride (**7i**)*

Yield: 85%; mp: 208–210 °C; IR (KBr) (ν_{max}/cm^{-1}): 3174 and 3047(2NH), 1671and 1639 (2C═O). ^{1}H NMR (DMSO-d_6, 500 MHz): δ (ppm) = 2.61 and 2.75 (t, J = 6.7 Hz, 4H, CH_2—CH_2), 4.54 (d, J = 5.7 Hz, 2H, CH_2—NH), 5.82 (s, 2H, —CH_2N^+), 7.32 (t, J = 7.5 Hz, 1H, H aromatic), 7.43 (t, J = 7.5 Hz, 2H, H aromatic), 7.49 (d, J = 8.5 Hz, 2H, H aromatic), 7.57 (d, J = 8.5 Hz, 2H, H aromatic), 7.61 (s, 1H, H_a thiazole), 7.90 (d, J = 7.5 Hz, 2H, H aromatic), 8.01 (d, J = 6.5 Hz, 2H, H_c,$H_{c'}$ pyridine), 8.80 (t, J = 5.8 Hz, 1H, N—H_1), 9.12 (d, J = 6.5 Hz, 2H, H_b,$H_{b'}$ pyridine), 12.30 (s, 1H, N—H_2). ^{13}C NMR (DMSO-d_6, 125 MHz): δ (ppm) = 29.6, 30.2, 41.6, 61.6, 107.8, 125.6, 125.8 127.7, 128.7, 129.2, 130.8, 133.3, 134.1, 134.2, 144.1, 148.7, 157.8, 160.5, 170.9, 172.0 (2C═O). MS (*m/z*, %): 491.2 (M^+, 100). Purity: 90%.

*4.2.10. 1-(2-Bromobenzyl)-4-((4-oxo-4-((4-phenylthiazol-2-yl)amino) butanamido)methyl) pyridin-1-ium bromide (**7j**)*

Yield: 80%; mp: 223–225 °C; IR(KBr) (ν_{max}/cm^{-1}): 3185 and 3052 (2NH), 1655 and 1639(2C═O). ^{1}H NMR (DMSO-d_6, 500 MHz): δ (ppm) = 2.62 and 2.76 (t, J = 6.7 Hz, 4H, CH_2—CH_2), 4.58 (d, J = 5.7 Hz, 2H, CH_2—NH), 5.92 (s, 2H, —CH_2N^+), 7.31–7.50 (m, 6H, H aromatic), 7.59 (s, 1H, H_a thiazole), 7.75 (d, J = 7.9 Hz, 1H, H aromatic), 7.90 (d, J = 7.5 Hz, 2H, H aromatic), 8.03 (d, J = 6.5 Hz, 2H, H_c,$H_{c'}$ pyridine), 8.83 (t, J = 5.7 Hz, 1H, N—H_1), 8.98 (d, J = 6.5 Hz, 2H, H_b,$H_{b'}$ pyridine), 12.31 (s, 1H, N—H_2). ^{13}C NMR (DMSO-d_6, 125 MHz): δ (ppm) = 29.4, 30.0, 41.6, 62.3, 107.9, 123.5, 125.7, 127.6, 128.7, 128.8, 129.5, 131.4, 131.6, 133.2, 133.5, 134.3, 144.6, 148.8, 157.9, 160.9, 171.0, 172.2 (2C═O). MS (*m/z*, %): 537.2 (M^+, 100). Purity: > 99%.

*4.2.11. 1-(3-Bromobenzyl)-4-((4-oxo-4-((4-phenylthiazol-2-yl)amino) butanamido)methyl) pyridin-1-ium bromide (**7k**)*

Yield: 75%; mp: 210–212 °C; IR (KBr) (ν_{max}/cm^{-1}): 3197 and 3043 (2NH), 1671and 1641(2C═O). ^{1}H NMR (DMSO-d_6, 500 MHz): δ (ppm) = 2.61 and 2.75 (t, J = 6.6 Hz, 4H, CH_2—CH_2), 4.55 (d, J = 5.7 Hz, 2H, CH_2—NH), 5.78 (s, 2H, —CH_2N^+), 7.32–7.53 (m, 5H, H aromatic), 7.60–7.63 (m, 2H, H_a thiazole, H aromatic), 7.82 (s, 1H, H aromatic), 7.90 (d, J = 7.5 Hz, 2H, H aromatic), 8.00 (d, J = 6.5 Hz, 2H, H_c,$H_{c'}$ pyridine), 8.77 (t, J = 5.8 Hz, 1H, N—H_1), 9.10 (d, J = 6.5 Hz, 2H, H_b,$H_{b'}$ pyridine), 12.30 (s, 1H, N—H_2). ^{13}C NMR (DMSO-d_6, 125 MHz) :δ (ppm) = 29.6, 30.2, 41.9, 61.9, 108.0, 122.5, 125.8, 126.1, 128.0, 128.1, 129.0, 131.6, 131.8, 132.5, 134.4, 136.9, 144.3, 148.9, 158.1, 160.8, 171.2, 172.4 (2C═O). MS (*m/z*, %): 537.2 (M^+, 100). Purity: > 99%.

*4.2.12. 1-(4-Bromobenzyl)-4-((4-oxo-4-((4-phenylthiazol-2-yl)amino) butanamido)methyl) pyridin-1-ium bromide (**7l**)*

Yield: 82%; mp: 221–223 °C; IR (KBr) (ν_{max}/cm^{-1}): 3180 and 3057 (2NH), 1670 and 1637 (2C═O). ^{1}H NMR(DMSO-d_6, 500 MHz): δ (ppm) = 2.60 and 2.75 (t, J = 6.5 Hz, 4H, CH_2—CH_2), 4.54 (d, J = 5.7 Hz, 2H, CH_2—NH), 5.79 (s, 2H, —CH_2N^+), 7.31–7.50 (m, 5H, H aromatic), 7.59–7.63 (m, 3H, H_a thiazole, H aromatic), 7.89 (d, J = 7 Hz, 2H, H aromatic), 8.00 (d, J = 5.0 Hz, 2H, H_c,$H_{c'}$ pyridine), 8.80 (t, J = 5.8 Hz, 1H, N—H_1), 9.10 (d, J = 5.0 Hz, 2H, H_b,$H_{b'}$ pyridine), 12.26 (s, 1H, N—H_2). ^{13}C NMR (DMSO-d_6, 125 MHz): δ (ppm) = 29.4, 30.0, 41.7, 61.8, 107.7, 122.8, 125.7, 125.9, 127.7, 128.8, 131.0, 132.1, 133.6, 134.3, 144.1, 148.7, 157.8, 160.5, 170.9, 172.0 (2C═O). MS (*m/z*, %): 537.2 (M^+, 100). Purity: 92%.

*4.2.13. 1-(2-Methylbenzyl)-4-((4-oxo-4-((4-phenylthiazol-2-yl)amino) butanamido)methyl) pyridin-1-ium bromide (**7m**)*

Yield: 70%; mp: 224–226 °C; IR (KBr) (ν_{max}/cm^{-1}): 3176 and 3028 (2NH), 1697 and 1654 (2C═O). ^{1}H NMR(DMSO-d_6, 500 MHz) :δ (ppm) = 2.27 (s, 3H, —CH_3), 2.61 and 2.75 (t, J = 6.7 Hz, 4H, CH_2—CH_2), 4.57 (d, J = 5.8 Hz, 2H, CH_2—NH), 5.86 (s, 2H, —CH_2N^+), 7.11 (d, J = 7.5 Hz, 1H, H aromatic), 7.25—7.33 (m, 4H, H aromatic), 7.43 (t, J = 7.7 Hz, 2H, H aromatic), 7.59 (s, 1H, H_a thiazole), 7.90 (d, J = 7.7 Hz, 2H, H aromatic), 8.01 (d, J = 6.5 Hz, 2H, H_c,$H_{c'}$ pyridine), 8.81 (t, J = 5.8 Hz, 1H, N—H_1), 8.92 (d, J = 6.5 Hz, 2H, H_b,$H_{b'}$ pyridine), 12.30 (s, 1H, N—H_2). ^{13}C NMR (DMSO-d_6, 125 MHz): δ (ppm) = 18.7, 29.5, 30.1, 41.6, 61.4, 108.4, 125.6, 125.7, 126.7, 127.7, 128.7, 129.0, 129.1, 129.3, 130.9, 132.3, 136.8, 144.8, 148.7, 157.9, 160.7, 170.9, 172.0 (2C═O). MS (*m/z*, %): 471.3 (M^+, 100). Purity: > 99%.

*4.2.14. 1-(3-Methylbenzyl)-4-((4-oxo-4-((4-phenylthiazol-2-yl)amino) butanamido)methyl) pyridin-1-ium chloride (**7n**)*

Yield: 68%; mp: 196–198 °C; IR (KBr) (ν_{max}/cm^{-1}): 3333 and 3178 (2NH), 1673 and 1606 (2C═O). ^{1}H NMR(DMSO-d_6, 500 MHz): δ (ppm) = 2.25 (s, 3H, —CH_3), 2.57 and 2.74 (t, J = 6.7 Hz, 4H, CH_2—CH_2), 4.58 (d, J = 5.9 Hz, 2H, CH_2—NH), 5.75 (s, 2H, —CH_2N^+), 7.25 (d, J = 5.0 Hz, 1H, H aromatic), 7.29–7.44 (m, 6H, H aromatic), 7.60 (s, 1H, H_a thiazole), 7.90 (d, J = 7.8 Hz, 2H, H aromatic), 8.01 (d, J = 6.5 Hz, 2H, H_c,$H_{c'}$ pyridine), 8.57 (t, J = 5.8 Hz, 1H, N—H_1), 9.11 (d, J = 6.5 Hz, 2H, H_b,$H_{b'}$ pyridine), 12.28 (s, 1H, N—H_2). ^{13}C NMR (DMSO-d_6, 125 MHz): δ (ppm) = 21.6, 29.6, 30.2, 41.0, 61.5, 107.8, 122.0, 125.6, 125.8, 127.7, 128.4, 128.7, 129.5, 129.7, 131.6, 134.3, 136.2, 144.6, 148.7, 157.9, 160.3, 170.9, 171.3 (2C═O). MS (*m/z*, %): 471.3 (M^+, 100). Purity: 92%.

*4.2.15. 1-(4-Methylbenzyl)-4-((4-oxo-4-((4-phenylthiazol-2-yl)amino) butanamido)methyl) pyridin-1-ium chloride (**7o**)*

Yield: 75%; mp: 208–210 °C; IR (KBr) (ν_{max}/cm^{-1}): 3333 and 3170 (2NH), 1673 and 1639 (2C═O). ^{1}H NMR(DMSO-d_6, 500 MHz): δ (ppm) = 2.24 (s, 3H, —CH_3), 2.60 and 2.74 (t, J = 6.3 Hz, 4H, CH_2—CH_2), 4.53 (d, J = 5.5 Hz, 2H, CH_2—NH), 5.76 (s, —CH_2N^+), 7.21 (d, J = 7.5 Hz, 2H, H aromatic), 7.24–7.45 (m, 5H, H aromatic), 7.61 (s, 1H, H_a thiazole), 7.91 (d, J = 7.0 Hz, 2H, H aromatic), 7.99 (d, J = 6.0 Hz, 2H, H_c,$H_{c'}$ pyridine), 8.91 (t, J = 5.5 Hz, 1H, N—H_1), 9.12 (d, J = 6.0 Hz, 2H, H_b,$H_{b'}$ pyridine), 12.30 (s, 1H, N—H_2). ^{13}C NMR (DMSO-d_6, 125 MHz): δ (ppm) = 20.7, 29.4, 30.2, 41.6, 62.4, 107.8,

122.0, 125.6, 125.7, 127.7, 128.7, 129.7, 131.4, 134.3, 138.9, 144.0, 148.7, 157.8, 160.3, 170.9, 171.3 (2C═O). MS (*m/z*, %): 471.3 (M^+, 100). Purity: 93%.

4.2.16. 1-(3-Methoxybenzyl)-4-((4-oxo-4-((4-phenylthiazol-2-yl)amino) butanamido)methyl) pyridin-1-ium chloride (**7p**)

Yield: 70%; mp: 199–201 °C; IR (KBr) (ν_{max}/cm^{-1}): 3333 and 3178 (2NH), 1674 and 1637 (2C═O). ^{1}H NMR(DMSO-d_6, 500 MHz): δ (ppm) = 2.60 and 2.74 (t, J = 6.5 Hz, 4H, CH_2—CH_2), 3.70 (s, 3H, —OCH_3), 4.54 (d, J = 5.5 Hz, 2H, CH_2—NH), 5.75 (s, 2H, —CH_2N^+), 6.97 (d, J = 8.0 Hz, 1H, H aromatic), 7.07 (d, J = 8.0 Hz, 1H, H aromatic), 7.16 (s, 1H, H aromatic), 7.25–7.45 (m, 4H, H aromatic), 7.61 (s, 1H, H_a thiazole), 7.90 (d, J = 7.5 Hz, 2H, H aromatic), 8.00 (d, J = 6.0 Hz, 2H, H_c,$H_{c'}$ pyridine), 8.85 (t, J = 5.0 Hz, 1H, N—H_1), 9.12 (d, J = 6.0 Hz, 2H, H_b,$H_{b'}$ pyridine), 12.30 (s, 1H, N—H_2). ^{13}C NMR (DMSO-d_6, 125 MHz): δ (ppm) = 29.5, 30.2, 41.6, 55.0, 62.5, 107.8, 112.7, 114.6, 120.5, 125.6, 125.7, 128.6, 128.8, 129.8, 131.6, 135.7, 144.1, 148.7, 157.5, 159.6, 160.8, 171.7, 172.6 (2C═O). MS (*m/z*, %): 487.3 (M^+, 100). Purity: > 99%.

4.2.17. 1-Benzyl-3-((4-oxo-4-((4-phenylthiazol-2-yl)amino)butanamido) methyl)pyridin-1-ium bromide (**7q**)

Yield: 75%; mp: 158–160 °C; IR (KBr) (ν_{max}/cm^{-1}): 3392 and 3193 (2NH), 1672 and 1557 (2C═O). ^{1}H NMR (DMSO-d_6, 500 MHz): δ (ppm) = 2.57 and 2.75 (t, J = 6.5 Hz, 4H, CH_2—CH_2), 4.48 (d, J = 5.5 Hz, 2H, CH_2—NH), 5.85 (s, 2H, —CH_2N^+), 7.32 (t, J = 7.5 Hz, 1H, H aromatic), 7.41–7.45 (m, 5H, H aromatic), 7.52 (d, J = 7 Hz, 2H, H aromatic), 7.59 (s, 1H, H_a thiazole), 7.89 (d, J = 7.5 Hz, 2H, H aromatic), 8.13 (t, J = 7.5 Hz, 1H, H_d pyridine), 8.49 (d, J = 7.5 Hz, 1H, H_c pyridine), 8.76 (t, J = 5.8 Hz, 1H, N—H_1), 9.09–9.11 (m, 2H, H_b,H_e pyridine), 12.32 (s, 1H, N—H_2). ^{13}C NMR (DMSO-d_6, 125 MHz): δ (ppm) = 29.4, 30.0, 41.1, 63.3, 107.7, 125.6, 127.7, 127.9, 128.6, 128.7, 129.1, 129.3, 134.1, 134.2, 141.1, 142.9, 143.1, 144.2, 148.7, 157.8, 170.9, 171.9 (2C═O). MS (*m/z*, %): 457.3 (M^+, 100). Purity: > 99%.

4.2.18. 1-(4-Nitrobenzyl)-3-((4-oxo-4-((4-phenylthiazol-2-yl)amino) butanamido)methyl) pyridin-1-ium bromide (**7r**)

Yield: 65%; mp: 203–205 °C; IR (KBr) (ν_{max}/cm^{-1}): 3347 and 3241 (2NH), 1658 and 1607 (2C═O). ^{1}H NMR (DMSO-d_6, 500 MHz): δ (ppm) = 2.57 and 2.75 (t, J = 7.0 Hz, 4H, CH_2—CH_2), 4.48 (d, J = 5.5 Hz, 2H, CH_2—NH), 6.02 (s, 2H, —CH_2N^+), 7.32 (t, J = 7.5 Hz, 1H, H aromatic), 7.42 (t, J = 7.5 Hz, 2H, H aromatic), 7.58 (s, 1H, H_a thiazole), 7.74 (d, J = 8.3 Hz, 2H, H aromatic), 7.89 (d, J = 7.5 Hz, 2H, H aromatic), 8.16 (t, J = 7.5 Hz, 1H, H_d pyridine), 8.28 (d, J = 8.3 Hz, 2H, H aromatic), 8.52 (d, J = 7.5 Hz, 1H, H_c pyridine), 8.77 (t, J = 5.5 Hz, 1H, N—H_1), 9.10–9.12 (m, 2H, H_b,H_e pyridine), 12.31 (s, 1H, N—H_2). ^{13}C NMR (DMSO-d_6, 125 MHz): δ (ppm) = 29.4, 30.0, 42.7, 62.3, 107.9, 124.1, 125.6, 127.8, 128.2, 128.7, 129.9, 131.6, 133.7, 134.3, 141.1, 141.3, 144.5, 147.6, 148.7, 157.8, 171.0, 172.1 (2C═O). MS (*m/z*, %): 502.3 (M^+, 100). Purity: > 99%.

4.2.19. 1-(4-Fluorobenzyl)-3-((4-oxo-4-((4-phenylthiazol-2-yl)amino) butanamido)methyl) pyridin −1-ium bromide (**7s**)

Yield: 62%; mp: 134–136 °C; IR (KBr) (ν_{max}/cm^{-1}): 3365 and 3203 (2NH), 1657 and 1604 (2C═O). ^{1}H NMR (DMSO-d_6, 500 MHz): δ (ppm) = 2.57 and 2.75 (t, J = 6.5 Hz, 4H, CH_2—CH_2), 4.47 (d, J = 5.0 Hz, 2H, CH_2—NH), 5.83 (s, 2H, —CH_2N^+), 7.27–7.44 (m, 5H, H aromatic), 7.59–7.63 (m, 3H, H_a thiazole, H aromatic), 7.89 (d, J = 7.6 Hz, 2H, H aromatic), 8.12 (t, J = 7.5 Hz, 1H, H_d pyridine), 8.47 (d, J = 7.5 Hz, 1H, H_c pyridine), 8.76 (t, J = 5.0 Hz, 1H, N—H_1), 9.08–9.10 (m, 2H, H_b,H_e pyridine), 12.31 (s, 1H, N—H_2). ^{13}C NMR (DMSO-d_6, 125 MHz): δ (ppm) = 29.5, 30.0, 42.6, 62.4, 107.8, 116.3 ($J_{C–F}$ = 21.6 Hz), 125.8, 127.5, 127.7, 128.9, 129.5, 130.9, 131.5, 133.6, 134.4, 141.8, 144.4, 149.0, 157.8, 161.3 ($J_{C–F}$ = 251.3 Hz), 171.0, 172.0 (2C═O). MS (*m/z*, %): 475.3 (M^+, 100). Purity: > 99%.

4.2.20. 1-(4-Chlorobenzyl)-3-((4-oxo-4-((4-phenylthiazol-2-yl)amino) butanamido)methyl) pyridin-1-ium bromide chloride (**7t**)

Yield: 68%; mp: 194–196 °C; IR (KBr) (ν_{max}/cm^{-1}): 3246 and 3065 (2NH), 1659 and 1599 (2C═O). ^{1}H NMR(DMSO-d_6, 500 MHz): δ (ppm) = 2.58 and 2.75 (t, J = 6.0 Hz, 4H, CH_2—CH_2), 4.47 (d, J = 4.5 Hz, 2H, CH_2—NH), 5.87 (s, 2H, —CH_2N^+), 7.32 (t, J = 7.5 Hz, 1H, H aromatic), 7.42 (t, J = 7.5 Hz, 2H, H aromatic), 7.51 (d, J = 7.8 Hz, 2H, H aromatic) , 7.59–7.63 (m, 3H, H_a thiazole, H aromatic), 7.88 (d, J = 7.5 Hz, 2H, H aromatic), 8.13 (t, J = 6.5 Hz, 1H, H_d pyridine), 8.50 (d, J = 6.5 Hz, 1H, H_c pyridine), 8.88 (t, J = 5.0 Hz, 1H, N—H_1), 9.13–9.15 (m, 2H, H_b,H_e pyridine), 12.33 (s, 1H, N—H_2). ^{13}C NMR (DMSO-d_6, 125 MHz): δ (ppm) = 29.4, 30.0, 41.1, 62.4, 107.7, 125.6, 127.7, 127.9, 128.6, 129.1, 130.7, 133.0, 134.1, 134.2, 141.1, 143.0, 143.1, 144.3, 148.7, 157.7, 170.9, 171.9 (2C═O). MS (*m/z*, %): 491.2 (M^+, 100). Purity: > 99%.

4.2.21. 1-(4-Bromobenzyl)-3-((4-oxo-4-((4-phenylthiazol-2-yl)amino) butanamido)methyl) pyridin-1-ium bromide bromide (**7u**)

Yield: 65%; mp: 138–140 °C; IR (KBr) (ν_{max}/cm^{-1}): 3306 and 3187 (2NH), 1699 and 1654 (2C═O). ^{1}H NMR(DMSO-d_6, 500 MHz): δ (ppm) = 2.58 and 2.75 (t, J = 6.4 Hz, 4H, CH_2—CH_2), 4.47 (d, J = 5.3 Hz, 2H, CH_2—NH), 5.84 (s ,2H, —CH_2N^+), 7.32 (t, J = 7.5 Hz, 1H, H aromatic), 7.43 (t, J = 7.5 Hz, 2H, H aromatic), 7.49 (d, J = 8.0 Hz, 2H, H aromatic) 7.59 (s, 1H, H_a thiazole), 7.65 (d, J = 8.0 Hz, 2H, H aromatic), 7.89 (d, J = 7.5 Hz, 2H, H aromatic), 8.13 (t, J = 7.5 Hz, 1H, H_d pyridine), 8.49 (d, J = 7.5 Hz, 1H, H_c pyridine), 8.75 (t, J = 5.7 Hz 1H, N—H_1), 9.08–9.10 (m, 2H, H_b,H_e pyridine), 12.31 (s, 1H, N—H_2). ^{13}C NMR (DMSO-d_6, 125 MHz): δ (ppm) = 29.5, 30.0, 42.3, 62.6, 107.8, 122.9, 125.6, 127.8, 128.1, 128.7, 129.6, 131.0, 132.1, 133.5, 134.3, 141.2, 143.2 144.3, 148.7, 157.8, 171.0, 172.0 (2C═O). MS (*m/z*, %): 537.2 (M^+, 100). Purity: > 99%.

4.3. Cholinesterase inhibition assay

Acetylcholinesterase (AChE, E.C. 3.1.1.7, Type V-S, lyophilized powder, from electric eel, 1000 units), butyrylcholinesterase (BChE, E.C. 3.1.1.8, from equine serum), and acetylthiocholine iodide were from Sigma-Aldrich. Reagent 5,5-dithiobis-(2-nitrobenzoic acid) (DTNB) from Sigma-Aldrich was kindly donated by Dr Y. Azarmi (Department of Pharmacology, Tabriz University of Medical Sciences, Tabriz, Iran). Disodium hydrogen phosphate was obtained from Fluka. Donepezil hydrochloride (Merck) used as the reference drug was kind gift from Darou Pakhsh Pharma Chem co, Tehran, Iran. The AChE and BChE inhibitory activity of synthesized compounds were determined by the modified spectroscopic method introduced by Ellman using acetylthiocholine iodide as the substrate in 96-well plates [59]. Derivatives and donepezil (the positive control) were dissolved in methanol (or a mixture of dimethyl sulfoxide (DMSO) and methanol) and then diluting in phosphate buffer adjusted at pH 8 to prepare the stock solutions. (Total amount of organic phase (DMSO and methanol) in each well was 0.5% at most.) Each compound was tested to inhibit the enzyme at different concentrations to achieve a range of inhibition between 20 and 80%. The assay solution consisted of 100 μL phosphate buffer (0.1 M, pH = 8), 30 μL DTNB (3.5 mM), 30 μL test compound solution and 20 μL of 2.5 U/mL AChE or BChE solution. The reaction was then initiated by adding 30 μL of acetylthiocholine iodide (7 mM) as the substrate to each well. The hydrolysis rate of acetylthiocholine was monitored at 412 nm by measuring the formation of yellow 5-thio-2-nitrobenzoate anion produced due to enzyme catalysis. The obtained

data were used to calculate IC_{50} values (mean ± S.E.) by GraphPad Prism (Version 6.01, 2012, GraphPad Software, Inc. USA). Each data point was the average of experiments in triplicate.

4.4. Kinetic studies of AChE inhibition

The reciprocal plots of 1/v versus 1/[S] were obtained by performing the AChE inhibition experiments at various concentrations of acetylthiocholine [S] and test compounds 7d and 7j using Ellman's method. The initial velocity (v) was determined based on the progress of the hydrolysis reaction monitored by absorbance change (ΔA) at 412 nm for 2 min and was expressed by ΔA/min. The slopes and ($1/v$)-axis intercepts of the reciprocal plots for each compound at different concentrations were used to generate secondary plots (slope and y-intercept replots). In slope replot, the slops of $1/v$ versus 1/[S] lines in the LWB plot were drawn against inhibitor concentration. In this replot, the slope is $K_m/(V_{max} \times K_i)$ and vertical intercept is K_m/V_{max} from which the K_i value was determined by vertical-axis intercept divided by the slope (i.e., the x-axis intercept equals $-K_i$). The K_i values were also determined using the nonlinear regression method implemented in GraphPad Prism (Version 6.01, 2012, GraphPad Software, Inc. USA) by analyzing the variation of velocity as a result of changes in the concentrations of both substrate and inhibitor. The factor α for the inhibition was determined using the y-intercept replot (also called ($1/v$)-intercept replot) where the abscissa intercept equals $-\alpha K_i$.

4.5. Inhibition of $A\beta_{1-42}$ self-induced aggregation

Inhibition of self-induced $A\beta_{1-42}$ aggregation of compounds **7a, 7d, 7g, 7j** and **7m** were measured using a thioflavin T (ThT)-based fluorometric assay method [64]. The Aβ sample (Anaspec Inc) as HFIP (hexafluoroisopropanol) pretreated $A\beta_{1-42}$ was dissolved in DMSO to give a 200 μM stock solution and then diluted in phosphate buffer (pH = 7.4, 50 mM) to obtain a 20 μM solution of $A\beta_{1-42}$ for the use in the assay. Compounds were dissolved in DMSO and diluted in the phosphate buffer to a final concentration of 20 μM. Then, the incubation of the peptide (final Aβ concentration = 10 μM, 10 μL) with and without inhibitor (final concentration = 10 μM, 10 μL) was performed at 30 °C for 48 h. After incubation, the prepared samples were diluted by 180 μL of 5 mM ThT in 50 mM glycine-NaOH buffer adjusted at pH 8.5 to the final volume of 200 μL. The fluorescence intensity was recorded on a microplate reader (Synergy HTX Multi-Mode Reader, BioTek Instruments) with excitation and emission wavelengths set at 440 nm and 485 nm, respectively. Each measurement was run in triplicates. Background fluorescence for a 5 mM ThT solution was subtracted from the intensities of the samples and the percent of aggregation inhibition was calculated according to equation (1- IF_i/IF_o) × 100% in which IF_i and IF_o are the fluorescence intensities obtained for Aβ in the presence and absence of inhibitor, respectively. The data were expressed as the average of measurements in triplicates.

4.6. Propidium iodide displacement assay

Propidium iodide is a compound that binds to PAS of AChE specifically. Being attached to the PAS of the enzyme, its fluorescence intensity increases up to eight folds. The compounds which are able to bind to the PAS could displace propidium iodide in a competitive manner leading to a decrease in fluorescence. This phenomenon implies that the compounds are PAS binders. 150 μL of 250 μM concentration of test compounds (final concentration = 93.75 μM) were added to 200 μL of 10U/mL of AChE (final concentration = 5U/mL) followed by 20 h incubation at 25 °C. Afterward, 50 μL propidium iodide 8 μM (final concentration = 1 μM) was added and the assay mixture was further incubated for 15 min. To justify the background signal, control wells containing all reagents except AChE were used as the blank solution. The decrease in fluorescence intensity was measured on a well plate reader mode with excitation at 535 nm and emission at 595 nm. Each compound was assayed in triplicate. Background intensity was subtracted from all the readings. The percent of fluorescence emission inhibition was calculated using the following formula: 100 – ($IF_i/IF_0 \times 100$), where IF_i and IF_0 are the fluorescence intensities with and without inhibitor, respectively.

4.7. Cell culture and MTT assay

PC_{12} cells were obtained from Pasteur Institute, Tehran, Iran, and cultured in DMEM supplemented with 10% fetal calf serum, 60 μg/mL penicillin, and 100 μg/mL streptomycin. To induce neuronal differentiation, the cells grown to 70% confluency were harvested by trypsin/EDTA (0.25%) solution and seeded in 96 well culture plate (4000 cells/well) and then cultured for one week in differentiation medium (DMEM + 2% horse serum + Nerve growth factor (NGF) (100 ng/ml) + penicillin and streptomycin). The effect of compounds **7a, 7d, 7g, 7j** and **7m** on the survival rate of PC_{12} neural cells were evaluated by changing the culture medium to NGF free medium and applying different concentrations of the compounds (1, 10 and 100 μg/mL) on cells. Donepezil (1, 10 and 100 μM) was used as the positive control. To apply the studied compounds at the required concentrations, their methanolic stock solutions were diluted in DMEM and a 10 μL volume was added to each well. Three hours later, apoptosis was induced by adding H_2O_2 (400 μM) to the medium followed by performing MTT assay after 12 h incubation. To each well was added a 10 μL MTT solution (5 mg/mL), and after 3.5 h, the medium was removed gently and 100 μL of the formazan solubilization solution containing 10% SDS in 0.01 M HCl (w/v) was added into each well. Then, the absorbance was measured at 570 nm with a reference wavelength of 630 nm using a plate reading spectrophotometer. The experiments were performed in triplicates. Culture media and supplements were from Gibco.

4.8. In vitro PAMPA-BBB assay

The *in vitro* brain permeability of the compounds was assessed by PAMPA-BBB assay described in literature with some modifications [67,68]. Test compounds were dissolved in DMSO at ~5 to 10 mg/mL and the stock solutions were diluted in PBS at pH 7.4 to get the final concentrations ~50 to 125 μg/mL. To each donor well was added 200 μL of the final solution. The filter membrane of the acceptor microplate (MultiScreen PAMPA filter plate, Millipore, kindly donated by Professor M. Foroutan from Faculty of Pharmacy, Shahid Beheshti University of Medical Sciences) was hydrated overnight in EtOH:PBS (3:7 V/V) and then was coated with 5 μL of soy lecithin lipid (lecithin, Carl Roth, kindly donated by Professor H. Valizadeh from Faculty of Pharmacy, Tabriz University of Medical Sciences) in dodecane (20 mg/mL). Subsequently, the acceptor well was filled with 200 μL of pH 7.4 PBS. The acceptor filter plate was placed on top of the donor plate to form a "sandwich", which then was incubated for 4 h to allow the diffusion of the test compound from the donor well into the acceptor well via lipid membrane. After incubation, the drug concentrations in acceptor and donor plates were determined by UV or fluorescent spectroscopy and the results were used to determine effective permeability (Pe) of the compounds. The experiment for each compound was performed in triplicates. Appropriate controls with known BBB permeability were also tested to validate the method. The integrity of the lipid membrane was evaluated using phenol red, a highly charged colored compound.

4.9. Docking studies

The 3D structures of the studied compounds were generated using Hyperchem software (version 8.0.8) and energy minimization using molecular mechanics (MM+) and semiempirical AM1 methods

[82,83]. Docking of the energy minimized structures into the binding site of the AChE (PDB code: 4EY7) was performed using the GOLD program (version 5.2.2, CCDC Software Limited) by applying ASP scoring function [73] and deselecting early termination option. The optimum docking condition was determined based on the results obtained for the docking of donepezil into the binding site of AChE and calculating the RMSD for the docking poses relative to the co-crystallized donepezil present in human AChE experimental structure 4EY7. The docking poses with the highest score for the two most active derivatives **7d** and **7j** were evaluated by PoseView and DeepView to investigate their mode of interactions with the enzyme.

Declaration of Competing Interest

The authors declare that they have no known competing financial interests or personal relationships that could have appeared to influence the work reported in this paper.

Acknowledgments

The authors would like to dedicate this paper to the memory of the late Professor Abbas Shafiee from Tehran University of Medical Sciences who contributed to the design of the project at the initial stages. We are grateful to Professor H. Nadri from Shahid Sadoughi University of Medical Sciences for his valuable assistance in performing propidium iodide displacement assay. We also would like to thank the Research Office and Biotechnology Research Center at Tabriz University of Medical Sciences for providing financial support under Postgraduate Research Scheme to the PhD thesis of GG (Grant number: 122).

Appendix A. Supplementary material

Supplementary data to this article can be found online at https://doi.org/10.1016/j.bioorg.2020.104186.

References

[1] B.D. James, S.E. Leurgans, L.E. Hebert, P.A. Scherr, K. Yaffe, D.A. Bennett, Contribution of Alzheimer disease to mortality in the United States, Neurology. 82 (2014) 1045–1050.
[2] T. Pan, S. Xie, Y. Zhou, J. Hu, H. Luo, X. Li, L. Huang, Dual functional cholinesterase and PDE4D inhibitors for the treatment of Alzheimer's disease: design, synthesis and evaluation of tacrine-pyrazolo [3, 4-b] pyridine hybrids, Bioorg. Med. Chem. Lett. 29 (2019) 2150–2152.
[3] T. Lazarevic-Pasti, A. Leskovac, T. Momic, S. Petrovic, V. Vasic, Modulators of acetylcholinesterase activity: from Alzheimer's disease to anti-cancer drugs, Curr. Med. Chem. 24 (2017) 3283–3309.
[4] M. Saxena, R. Dubey, Target enzyme in Alzheimer's disease: acetylcholinesterase inhibitors, Curr. Top. Med. Chem. 19 (2019) 264–275.
[5] J.M. Long, D.M. Holtzman, Alzheimer disease: an update on pathobiology and treatment strategies, Cell 179 (2019) 312–339.
[6] M. Zverova, Clinical aspects of Alzheimer's disease, Clin. Biochem. 72 (2019) 3–6.
[7] N. Braidy, A. Poljak, C. Marjo, H. Rutlidge, A. Rich, B.E. Jugder, T. Jayasena, N.C. Inestrosa, P.S. Sachdev, Identification of cerebral metal ion imbalance in the brain of aging octodon degus, Front. Aging. Neurosci. 9 (2017) 66.
[8] E. Koseoglu, New treatment modalities in Alzheimer's disease, World. J. Clin. Cases. 7 (2019) 1764–1774.
[9] L.-F. Lin, M.-J. Liao, X.-Y. Xue, W. Zhang, L. Yan, L. Cai, X.-W. Zhou, X. Zhou, H.-M. Luo, Combination of Aβ clearance and neurotrophic factors as a potential treatment for Alzheimer's disease, Neurosci. Bull. 29 (2013) 111–120.
[10] M. Rosini, E. Simoni, A. Milelli, A. Minarini, C. Melchiorre, Oxidative stress in Alzheimer's disease: are we connecting the dots? Miniperspective, J. Med. Chem. 57 (2013) 2821–2831.
[11] S. Agatonovic-Kustrin, C. Kettle, D.W. Morton, A molecular approach in drug development for Alzheimer's disease, Biomed. Pharmacother. 106 (2018) 553–565.
[12] J. Lalut, G. Santoni, D. Karila, C. Lecoutey, A. Davis, F. Nachon, I. Silman, J. Sussman, M. Weik, T. Maurice, Novel multitarget-directed ligands targeting acetylcholinesterase and σ1 receptors as lead compounds for treatment of Alzheimer's disease: Synthesis, evaluation, and structural characterization of their complexes with acetylcholinesterase, Eur. J. Med. Chem. 162 (2019) 234–248.
[13] H. Hampel, M.M. Mesulam, A.C. Cuello, M.R. Farlow, E. Giacobini, G.T. Grossberg, A.S. Khachaturian, A. Vergallo, E. Cavedo, P.J. Snyder, Z.S. Khachaturian, The cholinergic system in the pathophysiology and treatment of Alzheimer's disease, Brain. 141 (2018) 1917–1933.
[14] C.N. Pope, S. Brimijoin, Cholinesterases and the fine line between poison and remedy, Biochem. Pharmacol. 153 (2018) 205–216.
[15] V.K. Nuthakki, R. Mudududdla, A. Sharma, A. Kumar, S.B. Bharate, Synthesis and biological evaluation of indoloquinoline alkaloid cryptolepine and its bromo-derivative as dual cholinesterase inhibitors, Bioorg. Chem. 90 (2019) 103062.
[16] J. Avila, Our working point of view of tau protein, J. Alzheimer's Dis. 62 (2018) 1277–1285.
[17] L. Luo, Y. Li, X. Qiang, Z. Cao, R. Xu, X. Yang, G. Xiao, Q. Song, Z. Tan, Y. Deng, Multifunctional thioxanthone derivatives with acetylcholinesterase, monoamine oxidases and β-amyloid aggregation inhibitory activities as potential agents against Alzheimer's disease, Bioorg. Med. Chem. 25 (2017) 1997–2009.
[18] J. Sevigny, P. Chiao, T. Bussiere, P.H. Weinreb, L. Williams, M. Maier, R. Dunstan, S. Salloway, T. Chen, Y. Ling, J. O'Gorman, F. Qian, M. Arastu, M. Li, S. Chollate, M.S. Brennan, O. Quintero-Monzon, R.H. Scannevin, H.M. Arnold, T. Engber, K. Rhodes, J. Ferrero, Y. Hang, A. Mikulskis, J. Grimm, C. Hock, R.M. Nitsch, A. Sandrock, The antibody aducanumab reduces Abeta plaques in Alzheimer's disease, Nature 537 (2016) 50–56.
[19] G.K. Gouras, T.T. Olsson, O. Hansson, beta-Amyloid peptides and amyloid plaques in Alzheimer's disease, Neurotherapeutics. 12 (2015) 3–11.
[20] C.H. van Dyck, Anti-amyloid-β monoclonal antibodies for Alzheimer's disease: pitfalls and promise, Biol. Psychiatry. 83 (2018) 311–319.
[21] J.R. de Almeida, M. Figueiro, W.P. Almeida, C.H.T. de Paula da Silva, Discovery of novel dual acetylcholinesterase inhibitors with antifibrillogenic activity related to Alzheimer's disease, Future. Med. Chem. 10 (2018) 1037–1053.
[22] A. Alvarez, C. Opazo, R. Alarcon, J. Garrido, N.C. Inestrosa, Acetylcholinesterase promotes the aggregation of amyloid-beta-peptide fragments by forming a complex with the growing fibrils, J. Mol. Biol. 272 (1997) 348–361.
[23] A. Tripathi, P.K. Choubey, P. Sharma, A. Seth, P.N. Tripathi, M.K. Tripathi, S.K. Prajapati, S. Krishnamurthy, S.K. Shrivastava, Design and development of molecular hybrids of 2-pyridylpiperazine and 5-phenyl-1,3,4-oxadiazoles as potential multifunctional agents to treat Alzheimer's disease, Eur. J. Med. Chem. 183 (2019) 111707.
[24] P.N. Tripathi, P. Srivastava, P. Sharma, A. Seth, S.K. Shrivastava, Design and development of novel N-(pyrimidin-2-yl)-1,3,4-oxadiazole hybrids to treat cognitive dysfunctions, Bioorg. Med. Chem. 27 (2019) 1327–1340.
[25] R. Kumar, A. Nordberg, T. Darreh-Shori, Amyloid-beta peptides act as allosteric modulators of cholinergic signalling through formation of soluble BAbetaACs, Brain. 139 (2016) 174–192.
[26] R. Xu, G. Xiao, Y. Li, H. Liu, Q. Song, X. Zhang, Z. Yang, Y. Zheng, Z. Tan, Y. Deng, Multifunctional 5, 6-dimethoxybenzo [d] isothiazol-3 (2H)-one-N-alkylbenzylamine derivatives with acetylcholinesterase, monoamine oxidases and β-amyloid aggregation inhibitory activities as potential agents against Alzheimer's disease, Bioorg. Med. Chem. 26 (2018) 1885–1895.
[27] Y. Wang, H. Wang, H.Z. Chen, AChE Inhibition-based Multi-target-directed ligands, a novel pharmacological approach for the symptomatic and disease-modifying therapy of Alzheimer's disease, Curr. Neuropharmacol. 14 (2016) 364–375.
[28] F.J. Carvajal, N. Inestrosa Cantín, Interactions of AChE with Ab aggregates in Alzhemeirs brain; Therapeutic relevance of IDN 5706, Front. Mol. Neurosci. 4 (2011) 1–10.
[29] I.V. Zueva, V.E. Semenov, M.A. Mukhamedyarov, S.V. Lushchekina, A.D. Kharlamova, E.O. Petukhova, A.S. Mikhailov, S.N. Podyachev, L.F. Saifina, K.A. Petrov, O.A. Minnekhanova, V.V. Zobov, E.E. Nikolsky, P. Masson, V.S. Reznik, 6-Methyluracil derivatives as acetylcholinesterase inhibitors for treatment of Alzheimer's disease, Int. J. Risk. Saf. Med. 1 (2015) 69–71.
[30] E. Simoni, M. Bartolini, I.F. Abu, A. Blockley, C. Gotti, G. Bottegoni, R. Caporaso, C. Bergamini, V. Andrisano, A. Cavalli, I.R. Mellor, A. Minarini, M. Rosini, Multitarget drug design strategy in Alzheimer's disease: focus on cholinergic transmission and amyloid-beta aggregation, Future. Med. Chem. 9 (2017) 953–963.
[31] J.L. Cummings, G. Tong, C. Ballard, Treatment combinations for Alzheimer's disease: current and future pharmacotherapy options, J. Alzheimer's Dis. 67 (2019) 779–794.
[32] J. Wang, L. Tan, J.T. Yu, Prevention trials in Alzheimer's disease: current status and future perspectives, J. Alzheimer's Dis. 50 (2016) 927–945.
[33] M.M. Ibrahim, M.T. Gabr, Multitarget therapeutic strategies for Alzheimer's disease, Neural Regen. Res. 14 (2019) 437–440.
[34] P. Gonzalez-Naranjo, N.E. Campillo, C. Perez, J.A. Paez, Multitarget cannabinoids as novel strategy for Alzheimer disease, Curr. Alzheimer Res. 10 (2013) 229–239.
[35] M. Rosini, E. Simoni, R. Caporaso, A. Minarini, Multitarget strategies in Alzheimer's disease: benefits and challenges on the road to therapeutics, Future. Med. Chem. 8 (2016) 697–711.
[36] P. Sharma, P. Srivastava, A. Seth, P.N. Tripathi, A.G. Banerjee, S.K. Shrivastava, Comprehensive review of mechanisms of pathogenesis involved in Alzheimer's disease and potential therapeutic strategies, Prog. Neurobiol. 174 (2019) 53–89.
[37] S. Montanari, M. Bartolini, P. Neviani, F. Belluti, S. Gobbi, L. Pruccoli, A. Tarozzi, F. Falchi, V. Andrisano, P. Miszta, Multitarget Strategy to address Alzheimer's disease: design, synthesis, biological evaluation, and computational studies of coumarin-based derivatives, Chem. Med. Chem. 11 (2016) 1296–1308.
[38] M. Benchekroun, L. Ismaili, M. Pudlo, V. Luzet, T. Gharbi, B. Refouvelet, J. Marco-Contelles, Donepezil-ferulic acid hybrids as anti-Alzheimer drugs, Future. Med. Chem. 7 (2015) 15–21.
[39] D.G. van Greunen, C. Johan van der Westhuizen, W. Cordier, M. Nell, A. Stander, V. Steenkamp, J.L. Panayides, D.L. Riley, Novel N-benzylpiperidine carboxamide derivatives as potential cholinesterase inhibitors for the treatment of Alzheimer's disease, Eur. J. Med. Chem. 179 (2019) 680–693.
[40] P. Sharma, A. Tripathi, P.N. Tripathi, S.S. Singh, S.P. Singh, S.K. Shrivastava, Novel

molecular hybrids of N-Benzylpiperidine and 1,3,4-oxadiazole as multitargeted therapeutics to treat Alzheimer's disease, ACS Chem. Neurosci. 10 (2019) 4361–4384.
[41] M. Shidore, J. Machhi, K. Shingala, P. Murumkar, M.K. Sharma, N. Agrawal, A. Tripathi, Z. Parikh, P. Pillai, M.R. Yadav, Benzylpiperidine-linked diarylthiazoles as potential anti-Alzheimer's agents: synthesis and biological evaluation, J. Med. Chem. 59 (2016) 5823–5846.
[42] J. Cheung, M.J. Rudolph, F. Burshteyn, M.S. Cassidy, E.N. Gary, J. Love, M.C. Franklin, J.J. Height, Structures of human acetylcholinesterase in complex with pharmacologically important ligands, J. Med. Chem. 55 (2012) 10282–10286.
[43] R. Azzouz, L. Peauger, V. Gembus, M.L. Tintas, J. Sopkova-de Oliveira Santos, C. Papamicael, V. Levacher, Novel donepezil-like N-benzylpyridinium salt derivatives as AChE inhibitors and their corresponding dihydropyridine "bio-oxidizable" prodrugs: Synthesis, biological evaluation and structure-activity relationship, Eur. J. Med. Chem. 145 (2018) 165–190.
[44] J.S. Lan, J.W. Hou, Y. Liu, Y. Ding, Y. Zhang, L. Li, T. Zhang, Design, synthesis and evaluation of novel cinnamic acid derivatives bearing N-benzyl pyridinium moiety as multifunctional cholinesterase inhibitors for Alzheimer's disease, J. Enzyme. Inhib. Med. Chem. 32 (2017) 776–788.
[45] H. Chakravarty, Y. Ju, W.H. Chen, K.Y. Tam, Dual targeting of cholinesterase and amyloid beta with pyridinium/isoquinolium derivatives, Drug. Dev. Res. 81 (2020) 242–255.
[46] R.M. Sultanova, A.N. Lobov, A.V. Shumadalova, S.A. Meshcheryakova, Z.R. Zileeva, N.S. Khusnutdinova, V.A. Vakhitov, Y.V. Vakhitova, Synthesis of new 1,3-thiazol derivatives of maleopimaric acid as anticancer, antibacterial and antifungal agents, Nat. Prod. Res. (2019) 1–9.
[47] X.-D. Lin, H.-W. Yang, S. Ma, W.-W. Li, C.-H. Zhang, W.-J. Wang, R. Xiang, L.-L. Li, S.-Y. Yang, Discovery of 6-phenylimidazo [2, 1-b] thiazole derivatives as a new type of FLT3 inhibitors, Bioorg. Med. Chem. Lett. 25 (2015) 4534–4538.
[48] T.L. Schultz, C.P. Hencken, L.E. Woodard, G.H. Posner, R.H. Yolken, L. Jones-Brando, V.B. Carruthers, A thiazole derivative of artemisinin moderately reduces Toxoplasma gondii cyst burden in infected mice, J. Parasitol. 100 (2014) 516–521.
[49] A.K. Valiveti, U.M. Bhalerao, J. Acharya, H.N. Karade, B.N. Acharya, G. Raviraju, A.K. Halve, M.P. Kaushik, Synthesis and in vitro kinetic evaluation of N-thiazolylacetamido monoquaternary pyridinium oximes as reactivators of sarin, O-ethylsarin and VX inhibited human acetylcholinesterase (hAChE), Bioorg. Med. Chem. 23 (2015) 4899–4910.
[50] Z. Sahin, M. Ertas, C. Bender, E.F. Bulbul, B. Berk, S.N. Biltekin, L. Yurttas, S. Demirayak, Thiazole-substituted benzoylpiperazine derivatives as acetylcholinesterase inhibitors, Drug. Dev. Res. 79 (2018) 406–425.
[51] K. Matsueda, M. Hongo, J. Tack, H. Aoki, Y. Saito, H. Kato, Clinical trial: dose-dependent therapeutic efficacy of acotiamide hydrochloride (Z-338) in patients with functional dyspepsia - 100 mg t.i.d. is an optimal dosage, Neurogastroent, Motil. 22 (2010) 618–e173.
[52] Z.-Q. Sun, L.-X. Tu, F.-J. Zhuo, S.-X. Liu, Design and discovery of Novel Thiazole acetamide derivatives as anticholinesterase agent for possible role in the management of Alzheimer's, Bioorg. Med. Chem. Lett. 26 (2016) 747–750.
[53] J. Wang, C. Wang, Z. Wu, X. Li, S. Xu, J. Liu, Q. Lan, Z. Zhu, J. Xu, Design, synthesis, biological evaluation, and docking study of 4-isochromanone hybrids bearing N-benzyl pyridinium moiety as dual binding site acetylcholinesterase inhibitors (part II), Chem. Biol. Drug. Des. 91 (2018) 756–762.
[54] J.-S. Lan, Y. Ding, Y. Liu, P. Kang, J.-W. Hou, X.-Y. Zhang, S.-S. Xie, T. Zhang, Design, synthesis and biological evaluation of novel coumarin-N-benzyl pyridinium hybrids as multi-target agents for the treatment of Alzheimer's disease, Eur. J. Med. Chem. 139 (2017) 48–59.
[55] J. Joubert, G.B. Foka, B.P. Repsold, D.W. Oliver, E. Kapp, S.F. Malan, Synthesis and evaluation of 7-substituted coumarin derivatives as multimodal monoamine oxidase-B and cholinesterase inhibitors for the treatment of Alzheimer's disease, Eur. J. Med. Chem. 125 (2017) 853–864.
[56] A. Hiremathad, K. Chand, L. Tolayan, Rajeshwari, R.S. Keri, A.R. Esteves, S.M. Cardoso, S. Chaves, M.A. Santos, Hydroxypyridinone-benzofuran hybrids with potential protective roles for Alzheimer s disease therapy, J. Inorg. Biochem. 179 (2018) 82–96.
[57] M. Mostofi, G. Mohammadi Ziarani, M. Mahdavi, A. Moradi, H. Nadri, S. Emami, H. Alinezhad, A. Foroumadi, A. Shafiee, Synthesis and structure-activity relationship study of benzofuran-based chalconoids bearing benzylpyridinium moiety as potent acetylcholinesterase inhibitors, Eur. J. Med. Chem. 103 (2015) 361–369.
[58] N. Salehi, B.B.F. Mirjalili, H. Nadri, Z. Abdolahi, H. Forootanfar, A. Samzadeh-Kermani, T.T. Kucukkilinc, B. Ayazgok, S. Emami, I. Haririan, M. Sharifzadeh, A. Foroumadi, M. Khoobi, Synthesis and biological evaluation of new N-benzylpyridinium-based benzoheterocycles as potential anti-Alzheimer's agents, Bioorg. Chem. 83 (2019) 559–568.
[59] G.L. Ellman, K.D. Courtney, V. Andres Jr., R.M. Featherstone, A new and rapid colorimetric determination of acetylcholinesterase activity, Bio. Chem. Pharmacol. 7 (1961) 88–95.
[60] L.P. Hammett, The effect of structure upon the reactions of organic compounds. Benzene derivatives, J. Am. Chem. Soc. 59 (1937) 96–103.
[61] C. Hansch, T. Fojita, r-s-p Analysis. A method for the correlation of biological activity and chemical structure, J. Am. Chem. Soc. 86 (1964) 1616–1626.
[62] E.V. Anslyn, D.A. Dougherty, Modern Physical Organic Chemistry, University Science Books, Sausalito, California, 2006.
[63] F. Rahim, M.T. Javed, H. Ullah, A. Wadood, M. Taha, M. Ashraf, A. Qurat ul, M.A. Khan, F. Khan, S. Mirza, K.M. Khan, Synthesis, molecular docking, acetylcholinesterase and butyrylcholinesterase inhibitory potential of thiazole analogs as new inhibitors for Alzheimer disease, Bioorg. Chem. 62 (2015) 106–116.
[64] M. Bartolini, C. Bertucci, M.L. Bolognesi, A. Cavalli, C. Melchiorre, V. Andrisano, Insight into the kinetic of amyloid β (1–42) peptide self-aggregation: elucidation of inhibitors' mechanism of action, Chem. Bio. Chem. 8 (2007) 2152–2161.
[65] P. Sharma, A. Tripathi, P.N. Tripathi, S.K. Prajapati, A. Seth, M.K. Tripathi, P. Srivastava, V. Tiwari, S. Krishnamurthy, S.K. Shrivastava, Design and development of multitarget-directed N-Benzylpiperidine analogs as potential candidates for the treatment of Alzheimer's disease, Eur. J. Med. Chem. 167 (2019) 510–524.
[66] M. Estrada Valencia, C. Herrera-Arozamena, L. de Andres, C. Perez, J.A. Morales-Garcia, A. Perez-Castillo, E. Ramos, A. Romero, D. Vina, M. Yanez, E. Laurini, S. Pricl, M.I. Rodriguez-Franco, Neurogenic and neuroprotective donepezil-flavonoid hybrids with sigma-1 affinity and inhibition of key enzymes in Alzheimer's disease, Eur. J. Med. Chem. 156 (2018) 534–553.
[67] L. Di, E.H. Kerns, K. Fan, O.J. McConnell, G.T. Carter, High throughput artificial membrane permeability assay for blood-brain barrier, Eur. J. Med. Chem. 38 (2003) 223–232.
[68] A. Seth, P.A. Sharma, A. Tripathi, P.K. Choubey, P. Srivastava, P.N. Tripathi, S.K. Shrivastava, Design, synthesis, evaluation and molecular modeling studies of some novel N-substituted piperidine-3-carboxylic acid derivatives as potential anticonvulsants, Med. Chem. Res. 27 (2018) 1206–1225.
[69] G.L. Waldrop, A qualitative approach to enzyme inhibition, Biochem. Mol. Biol. Edu. 37 (2009) 11–15.
[70] I.H. Segel, Enzyme kinetics: behavior and analysis of rapid equilibrium and steady state enzyme systems, (1975).
[71] Y. Bourne, J. Grassi, P.E. Bougis, P. Marchot, Conformational flexibility of the acetylcholinesterase tetramer suggested by x-ray crystallography, J. Biol. Chem. 274 (1999) 30370–30376.
[72] G. Santoni, J. de Sousa, E. de la Mora, J. Dias, L. Jean, J.L. Sussman, I. Silman, P.Y. Renard, R.C.D. Brown, M. Weik, R. Baati, F. Nachon, Structure-based optimization of nonquaternary reactivators of acetylcholinesterase inhibited by organophosphorus nerve agents, J. Med. Chem. 61 (2018) 7630–7639.
[73] W.T. Mooij, M.L. Verdonk, General and targeted statistical potentials for protein–ligand interactions, Proteins. 61 (2005) 272–287.
[74] R. Caliandro, A. Pesaresi, L. Cariati, A. Procopio, M. Oliverio, D. Lamba, Kinetic and structural studies on the interactions of Torpedo californica acetylcholinesterase with two donepezil-like rigid analogues, J. Enzyme. Inhib. Med. Chem. 33 (2018) 794–803.
[75] O.J. Olatunji, A.L. Ogundajo, I.A. Oladosu, K. Changwichit, K. Ingkaninan, S. Yuenyongsawad, A. Plubrukarn, Non-competitive inhibition of acetylcholinesterase by bromotyrosine alkaloids, Nat. Prod. Commun. 9 (2014) 1559–1561.
[76] S.M. Rizvi, S. Shaikh, D. Naaz, S. Shakil, A. Ahmad, M. Haneef, A.M. Abuzenadah, Kinetics and molecular docking study of an anti-diabetic drug glimepiride as acetylcholinesterase inhibitor: implication for Alzheimer's disease-diabetes dual therapy, Neurochem. Res. 41 (2016) 1475–1482.
[77] C.A. Lipinski, F. Lombardo, B.W. Dominy, P.J. Feeney, Experimental and computational approaches to estimate solubility and permeability in drug discovery and development settings, Adv. Drug. Deliv. Rev. 46 (2001) 3–26.
[78] W.J. Egan, K.M. Merz Jr., J.J. Baldwin, Prediction of drug absorption using multivariate statistics, J. Med. Chem. 43 (2000) 3867–3877.
[79] I. Muegge, S.L. Heald, D. Brittelli, Simple selection criteria for drug-like chemical matter, J. Med. Chem. 44 (2001) 1841–1846.
[80] A.K. Ghose, V.N. Viswanadhan, J.J. Wendoloski, A knowledge-based approach in designing combinatorial or medicinal chemistry libraries for drug discovery. 1. A qualitative and quantitative characterization of known drug databases, J. Comb. Chem. 1 (1999) 55–68.
[81] D.F. Veber, S.R. Johnson, H.Y. Cheng, B.R. Smith, K.W. Ward, K.D. Kopple, Molecular properties that influence the oral bioavailability of drug candidates, J. Med. Chem. 45 (2002) 2615–2623.
[82] M.J.S. Dewar, W. Thiel, Ground states of molecules. 39. MNDO results for molecules containing hydrogen, carbon, nitrogen, and oxygen, J. Am. Chem. Soc. 99 (1977) 4907–4917.
[83] N.L. Allinger, Conformational analysis. 130. MM2. A hydrocarbon force field utilizing V1 and V2 torsional terms, J. Am. Chem. Soc. 99 (1977) 8127–8134.